MOLECULAR VIBRATIONS AND MOLECULAR DIMENSIONS IN SOME LARGE MOLECULAR SYSTEMS

BY

BASANTI LAL DEOPURA

PHY
1971
D
DEO

Th
Phy 1971/D
D44m

DEPARTMENT OF PHYSICS

INDIAN INSTITUTE OF TECHNOLOGY KANPUR

JUNE 1971

MOLECULAR VIBRATIONS AND MOLECULAR DIMENSIONS IN SOME LARGE MOLECULAR SYSTEMS

A Thesis Submitted
In Partial Fulfilment of the Requirements
for the Degree of
DOCTOR OF PHILOSOPHY

BY
BASANTI LAL DEOPURA

to the

DEPARTMENT OF PHYSICS
INDIAN INSTITUTE OF TECHNOLOGY KANPUR

JUNE 1971

22153

PHY-1971-D-DEO-MO JU F'76

CERTIFICATE

Certified that this work on "Molecular Vibrations and Molecular Dimensions in Some Large Molecular Systems" by B.L. Deopura has been carried out under my supervision and that this has not been submitted elsewhere for a degree.

(V.D. GUPTA)
Assistant Professor
Department of Physics
Indian Institute of Technology Kanpur

ACKNOWLEDGEMENTS

I wish to express a deep sense of gratitude to Professor V.D. Gupta for suggesting the problem and for his kind encouragement and stimulating guidance throughout the course of this work.

My thanks are due to Professor J. Mahanty and Dr. R.C. Srivastava for their kind interest in the work.

I am indebted to the scientists at the Army Materials and Mechanics Research Centre, U.S.A., for obtaining the neutron spectrum of Triamino-Trinitrobenzene and to Mr. H.K. Sehgal of Indian Institute of Technology, Delhi, for his help in recording the Raman spectrum. I am thankful to Mr. N.R. Yadav for his help during small-angle X-ray scattering experiments and to several other friends for their timely help.

The facilities provided at the Computer Centre, IIT-Kanpur are gratefully acknowledged.

I wish to thank Mr. M. Natu for patient and careful typing of the thesis, and Mr. H.K. Panda for cyclostyling the same.

The research was supported in part by a grant from the U.S. Department of Agriculture under PL-480, which is gratefully acknowledged.

B.L. Deopura

TABLE OF CONTENTS

LIST OF TABLES

LIST OF FIGURES AND PLATES

SYNOPSIS

MOLECULAR VIBRATIONS AND MOLECULAR DIMENSIONS IN SOME LARGE MOLECULAR SYSTEMS

B.L. DEOPURA
Ph.D.
Department of Physics
Indian Institute of Technology Kanpur
June 1971

The thesis is concerned with the vibrational studies of 1,3,5-Triamino-2,4,6-Trinitrobenzene (TATNB) and a study of low-angle X-ray scattering from polyethylene before and after irradiation. In the former a complete normal mode analysis including evaluation of thermodynamic quantities and mean square amplitudes has been carried out. Infrared absorption, Raman scattering and inelastic neutron scattering are used as tools of molecular spectroscopy. The X-ray scattering at low-angles from polyethylene is analysed on the basis of a two-phase model and position correlation functions are obtained. The peak positions are compared with the electron microscopic observations.

The first chapter forms a general introduction to the thesis, the importance of vibrational analysis in regard to the assignments of the observed frequencies and detailed spatial nature of the vibrations of a molecule is discussed.

Such studies are very useful in case of macromolecular systems with various conformations. The study of low-angle scattering is important for two main reasons. First, it can provide information on how the macromolecular chains are organised into the large scale units. Second, in some cases it may be possible to obtain information about the internal structure. Further, low - angle X-ray scattering could give information regarding the crystallite size, orientation, degree of order etc.

The second chapter of the thesis is concerned with the theoretical approach used for the treatment of the normal vibrations of a finite molecule. It is based on Wilson's GF matrix method. The usefulness of group theoretical principles in factoring the dynamical matrix and in classification of various normal modes is discussed. In addition to infrared absorption and Raman scattering, inelastic neutron scattering is also an important tool of molecular spectroscopy. It is because inelastic neutron scattering is not limited by symmetry dependent selection rules and as such in principle should provide 'complete' information about a vibrating system. The theoretical principles involved are outlined in this chapter.

The third chapter deals with the analysis of the TATNB molecule based on Wilson's method. Factor group analysis is based on D_{3h} point group symmetry. The assignments of the observed frequencies are made on the basis of potential energy

distribution, symmetry principles, peak intensities, bond orders and group frequencies. In neutron spectrum the fact that the intensities of various peaks are weighted by the square of the amplitude of motion of the protons is used. NH_2 and NO_2 group modes, X-sensitive modes and ring modes are discussed in details. Urey-Bradley force field is obtained. Spatial representation of a few important normal modes is presented. The thermodynamic parameters are evaluated.

The next chapter gives the theoretical details regarding X-ray scattering studies at low-angles. A two-phase electron density model for semicrystalline polyethylene is presented. A layer-like structure is considered. Theoretical correlation function from the autoconvolution of the electron density variations in the sample-model is calculated. It can be compared with the experimental correlation function obtained from fourier transform of the scattering curve. The variables of the model (crystalline and amorphous lengths and the widths of the distribution functions) are varied to match the theoretical curve with the experimental one.

In the fifth chapter experimental and theoretical studies on low - angle scattering from a polyethylene sample which has been annealed just below the melting point and cooled very slowly to room temperature are presented. Luzzati-Baro camera is used and for slit height correction, the slit was regarded as infinite. The position of the first maximum at 118 a.u.

agrees with the electron microscopic observations. In order to test the validity of a clear-cut two phase model, studies are made on neutron irradiated sample. Since irradiation brings about cross-linking, the analysis of the experimental curve is complicated because the cross-linked regions could have a higher electron density and the distribution of layer thicknesses in two phases is broadened. Finally, theoretical calculations for a layer-structure and two phase model are made to fit the experimental correlation curves. Normal distribution functions for the average lengths of the crystalline and amorphous regions are used. The model parameters are reported. Preliminary observations on low-angle X-ray scattering from wool are also given.

The last chapter of the thesis deals with the approximations involved in the work and outlines a programme for further work. Since TATNB is insoluble in almost all the solvents, the spectra are obtained in the solid state. This necessitates calculations for a three dimensional system taking into account all intermolecular interactions and further one has to consider space group symmetry for determining optical activity and symmetry species of different modes. For low-angle scattering the present two phase model is certainly not the best because in practice a clear-cut demarcation between ordered and disordered phase is impossible to make. It is expected that a model with more phases would yield better results These and several other limitations are discussed in this concluding part of the thesis.

CHAPTER - I

INTRODUCTION

A study of the normal modes of vibrations of a molecule is interesting not only in knowing the nature of the vibrations taking place but also in understanding the thermodynamic properties of the system. The numerical value of a vibrational frequency is chiefly a function of the magnitude of binding (force constants) among the constituent atoms and their masses, whereas the physical nature of a vibration depends mainly on the symmetry properties of the molecule. If the symmetry and roughly the nature of bonding, not the magnitude, are known in a molecule, the physical nature of the normal vibrations can be understood, and thus some of the spatial characteristics can be elucidated, like the direction in which electric moment, if any, changes during a vibration and therefore the selection rules, the degeneracy of the normal modes etc.

Infrared absorption and Raman scattering are mostly used as tools of molecular spectroscopy and the assignments of the observed peaks without normal mode calculations, is done primarily on the basis of group frequencies and thus remains somewhat arbitrary. It may not be so bad for small molecules. The experimental information itself is generally incomplete because several peaks may not be observed either because symmetry dependent selection rules do not allow

them or else they are too weak to be seen in the spectrum. A complete vibrational analysis of a molecule leads to all the internal modes and it is possible to obtain details about the nature of displacements of various atoms in each mode[1,2]. More important, the potential energy distribution in various degrees of freedom enables a definite assignment of the modes observed. The assignments of the group frequencies in model-compounds and identical environmentsare also very helpful in such studies.

Recently, much work has been done on the vibrational analysis of long-chain helical macromolecules[3-5], where the vibrations of adjacent units are related through a phase-factor. Conformational sensitive modes and their dispersion are calculated. From the dispersion curves a one dimensional phonon distribution function is obtained.

For 1,3,5-triamino-2,4,6-trinitrobenzene (TATNB), molecules such as s-trinitrobenzene, aniline, p-nitroaniline could be regarded as model-compounds. They provide useful initial information for vibrational analysis of TATNB. There are, however, several ambiguities and inconsistencies in the assignments of peak positions observed in infrared absorption and Raman scattering in these systems[6-8]. These and transferability of force constants are discussed in details in Chapter III.

A study of small-angle X-ray scattering[9-11] from macromolecular systems is of importance for two main reasons. First, it provides information on the organization of macromolecular chains and secondly, in some cases it is possible to obtain information about the internal structure of the element associated with the small-angle scattering, since the transform of the element may determine some features of this scattering. For example, the discrete equatorial diffraction maxima can arise from either inter-unit interference or intra-unit interference in a unit containing a small number of fibrous elements. In the first case the distance between the centres of units is assumed large enough that the first order diffraction maximum occurs at a value of $(2 \sin \theta / \lambda)$, which is of the order of $1/r$ where r is the distance between the centres of the units, 2θ is the scattering angle and λ is the wave length of the radiation. In the second case units are considered to scatter independently and the maxima at small angles arise from the lack of extended lateral order.

With the common small-angle scattering apparatus, the scattered intensity can be measured only on a relative scale. A great improvement is achieved when the scattered beam is measured on an absolute scale i.e. when the scattered intensity is compared to the energy of the primary beam. In this case it is possible to determine several additional

parameters, such as molecular weight and internal hydration in the case of a solution of globular particles[12]. For helical macromolecules in solution which behave like rigid rods it is possible to determine linear mass of the rods and repeat distance[13]. Because of the great interest in linear polypeptides and nuclic-acid structure, such measurements are most fruitful as regard to their conformational analysis.

Small-angle X-ray scattering studies cannot provide any detailed and exhaustive description of the system and one has to contend with average characteristic parameters. Specially, in cases where polydispersity or high anisotropy of the particle is present, one can obtain only a statistical average for the size and shape.

In the work outlined in Chapter IV and V, small-angle X-ray scattering from a well annealed polyethylene sample is presented. Small-angle studies for polyethylene are reported by several earlier workers[14-18]. However, their work has been mostly confined to measurement of long periods in fibrous and melt-crystallized samples. Recently, Vonk[19,20] et al. have reported a study of correlation functions based on a two-phase parallel layer model with different average electron densities. However, their results vary within wide limits. The problem has been restudied by carefully taking into account the history of the sample. The experimental correlation function is obtained by fourier transforming the

scattering curve. The position correlation functions have an important advantage over the direct analysis of the scattering curve. Interparticle interferences are automatically taken care of in the former approach. These effects are very important in solid state.

REFERENCES

1. E.B. Wilson, Jr., J. Chem. Phys. 7, 1047 (1939); 9, 76 (1941); E.B. Wilson, Jr., J.C. Decius and P.C. Cross, "Molecular Vibrations", McGraw-Hill, New York (1955).

2. S.J. Syvin, "Molecular Vibrations and Mean Square Amplitudes", Elsevier Publishing Company, Amsterdam (1968).

3. T. Miyazawa, J. Chem. Phys. 35, 693 (1961); T. Miyazawa, K. Fukushima and Y. Ideguchi, J. Chem. Phys. 37, 2764 (1962); T. Miyazawa, Y. Ideguchi and K. Fukushima, J. Chem. Phys. 38, 2709 (1963).

4. M.V. Krishnan and V.D. Gupta, Chem. Phys. Letters 6, 231 (1970).

5. V.D. Gupta, S. Trevino and H. Boutin, J. Chem. Phys. 48, 3008 (1968); R.D. Singh and V.D. Gupta, Spectrochim. Acta 27A, 385 (1971).

6. J.C. Evans, Spectrochim. Acta 16, 428 (1960).

7. J. Brandmüller, E.W. Schmid, H.W. Schröter and G. Nonnenmacher, Spectrochim. Acta 17, 523 (1961).

8. H.F. Shurvell, J.A. Faniran, E.A. Symons and E. Buricel, Can. Jou. Chemistry 45, 117 (1967).

9. A. Guinier and G. Fournet, "Small-angle scattering of X-rays", John Wiley, New York (1955).

10. H. Brumberger (Ed.), "Small-Angle X-Ray Scattering", Gordon and Breach, New York (1967).

11. R. Hosemann, A. Schönfeld, W. Wilke in "Advances in Structural Research by Diffraction Methods", Ed. R. Brill and R. Mason, Fergamon Press, Oxford (1970).

12. V. Luzzati, Acta Cryst. 13, 939 (1960).

13. V. Luzzati, A. Nicalaieff and F. Masson, J. Mol. Biol. 3, 185 (1961); V. Luzzati, D. Luzzati and F. Masson, J. Mol. Biol. 5, 375 (1962).

14. W.O. Statton, J. Polymer Sci. 28, 423 (1958).

15. A. Keller, Kolloid Z.u.Z. Polymere 165, 34 (1959).

16. P.H. Geil, J. Polymer Sci. C13, 149 (1966).

17. R. Hosemann, W. Wilke and F.J. Balta Colleja, Acta Cryst. 21, 118 (1966).

18. D. Ya. Tsvankin, Vysokomol. Soedin. Ser. A9, 2668 (1967).

19. C.G. Vonk and G. Kortleve, Kolloid Z. u. Z. Polymere 220, 19 (1967).

20. G. Kortleve and C.G. Vonk, Kolloid Z. u. Z. Polymere 225, 124 (1968).

CHAPTER - II

THEORY OF MOLECULAR VIBRATIONS

MOLECULAR VIBRATIONS

In this section a treatment of the molecular dynamics of finite molecules is presented. A molecule with N atoms has (3N-6) or (3N-5) vibrational degrees of freedom depending on whether it is non-linear or linear. The six non-genuine degrees of freedom are associated with free translations and rotations of the molecule. For a linear molecule, the rotational degrees of freedom are only two. Corresponding to these (3N-6) or (3N-5) vibrational degrees of freedom, there are as many fundamental normal modes of vibration. All other modes are linear combinations of them. The Wilson GF matrix[1,2] method is mostly used for calculating the normal modes of vibration. In this method 'internal coordinates' are used to describe the motion; these are changes in bond lengths, bond angles; out-of-plane wags and torsional motions. Physical nature of the vibration can be easily visualized in terms of internal coordinates. It also enables one to transfer force constants from a group in a molecule to a group in another in similar environment. The molecular vibrations are assumed to be small and harmonic and thus transformations between various displacement coordinates are linear. They are easily expressed in matrix notation. The transformation of cartesian coordinates X to internal coordinates R is

expressed as

$$R = BX \qquad (2.1)$$

B is the matrix of transformation. The kinetic energy in terms of internal coordinates is given by

$$2T = \dot{R}' G^{-1} \dot{R} \qquad (2.2)$$

R' is the transpose of R. The G-matrix or inverse kinetic energy matrix in terms of B matrix is written as

$$G_{kl} = \sum_{i=1}^{3N} B_{ki} B_{li} / m_i \quad (k = 1,2,\ldots,3N-6) \qquad .. \quad (2.3)$$

where m_i is the mass of the i^{th} atom, n is the number of atoms.

Potential energy is given by the relation

$$2V = R' FR \qquad (2.4)$$

where F is the potential energy matrix and is related to force constants through Z-matrix by the relation[3]

$$F_{ij} = \sum_{k} Z_{ijk} f_k \qquad (2.5)$$

The problem of molecular vibrations then reduces to the following secular equation

$$|GF - E\lambda| = 0 \qquad (2.6)$$

λ's are the eigenvalues relate to the vibrational frequencies ν by the relation $\lambda_k = 4\pi^2\nu_k^2 c^2$. Normal coordinates Q are related to internal coordinates R by the matrix L as

$$R = LQ \qquad (2.7)$$

where the column vectors L are given by the relation

$$(GF)L = \lambda L \qquad (2.8)$$

The solution of the above equation yields the eigenvector L of the dynamical matrix.

A measure of the nature of the normal vibrations (mixing of various modes) is the fractional potential energy associated with each internal coordinate. The fractional potential energy of the k^{th} normal mode associated with i^{th} internal coordinate is given by[4]

$$(P.E.)_i^k = L_{ik} F_{ii} / \lambda_k \qquad (2.9)$$

The potential energy distribution is useful in making assignments of various frequencies.

SYMMETRY PRINCIPLES

The importance of the symmetry of the molecule and group theoretical ideas may be mentioned at this point. The symmetry and geometry of the molecular-model can be used to determine the number of normal modes belonging to different

symmetry species of the molecular point group, selection rules for infrared absorption and Raman scattering, factorization of the secular equation and other useful information.

The number of normal modes in a given symmetry species 'γ' of the point group is given by the relation[2]

$$\eta(\gamma) = \frac{1}{g} \sum_{R} \chi_R(\gamma)^* \chi_R \qquad (2.10)$$

g is the number of symmetry operations and sum is over all such operations. $\chi_R(\gamma)$ is the character of the 'γ' symmetry species, for the operation R. Characters χ_R can be written as

$$\chi_R = \sum_{i} R_{ii} \qquad (2.11)$$

in which R_{ii} are the diagonal coefficients, in the transformation

$$q_i' = \sum_{j=1}^{3N} R_{ij} q_j \qquad (2.12)$$

which corresponds to symmetry operation R. q_j and q_i' are the displacement coordinates before and after the symmetry operation. From relation (2.11) and (2.12) it follows that χ_R can be found by the number of unshifted atoms with an appropriate multiplicative factor[2] of the symmetry operation.

Symmetry considerations can also predict the modes which will be allowed in infrared absorption and Raman

scattering. In the former case, the intensity is governed by the changes in dipole moment whereas in the latter case, it is dependent on changes in polarizability. In a given symmetry point group the three components of the dipole moment transforms according to one of the species and the normal modes belonging to these species will be infrared active with the corresponding polarizations. Similar consideration applies for changes in the six polarizability components and Raman activity of the normal modes.

As mentioned earlier, the symmetry of the molecule can be exploited in solving the secular equation by transforming the kinetic and potential energy matrices in the space of symmetry coordinates. These are written as linear combinations of the internal coordinates with coefficients obtained from the Character Table of the molecular point group. For a non-degenerate symmetry species the symmetry coordinate $S^{(\gamma)}$ can be written down as

$$S^{(\gamma)} = N \sum_{R} \chi_R^{(\gamma)} RS_1 \qquad (2.13)$$

$\chi_R^{(\gamma)}$ is same as in equation (2.10). Notation RS_1 stands for the coordinate, to which the displacement of the originally used coordinate S_1 is transformed by the operation R. Sum is over all the symmetry operations. N is the normalization factor. Each symmetry coordinate belongs to one of the symmetry species and in a way represents a normal

mode. The dynamical matrix when transformed in the space of symmetry coordinates, factors in a block diagonal structure, each of these blocks belongs to one of the symmetry species. Let 'U' represent the transformation matrix between internal coordinates R and symmetry coordinates S then

$$S = UR \tag{2.14}$$

The U-matrix is used to get the block diagonal form of G and F matrices by similarity transformation:

$$\begin{aligned} G^B &= U' G U \\ F^B &= U' F U \end{aligned} \tag{2.15}$$

U is a real matrix. U' is the transpose of U. The secular equation (2.6) reduces to the form $\left| G^{(\gamma)} F^{(\gamma)} - E \lambda \right| = 0$. These can be solved completely independent of each other for individual symmetry species.

MEAN SQUARE AMPLITUDES

A mean square amplitude matrix $\sum$ is defined as

$$\sum = R R^{\dagger} \tag{2.16}$$

R is a set of coordinates for the molecule. $R^{\dagger}$ represents the trans-conjugate of R. In general, a mean square amplitude matrix (2.16) can be constructed using the coordinates which need not necessarily be complete or

independent[5]. A set of conventional valence coordinates can be fruitfully used. The transformation matrix L between normal coordinates Q and internal coordinates R can be expressed in the form:

$$R_i = \sum_k L_{ik} Q_k \qquad (2.17)$$

The $\sum$ matrix equation (2.16) expressed in terms of normal coordinates is

$$\sum = L \langle Q_k Q_k^+ \rangle . L^+ \qquad (2.18)$$

or

$$\sum = L \delta L^+ \qquad (2.19)$$

where

$$\delta = \langle Q_k Q_k^+ \rangle$$

using the harmonic oscillator model, we get[5]

$$\langle Q Q^+ \rangle = \frac{h}{4\pi^2 c \omega} \operatorname{Coth} (hc\omega/2kT) \qquad (2.20)$$

ω is the frequency of the oscillator, T is the absolute temperature. The elements of $\sum$ matrix for a given normal mode k can be written down as

$$\sum_{ij} = \sum_k L_{ik} L^*_{jk} \delta_k \qquad (2.21)$$

These quantities are independent of the special set of internal coordinates which might have been used in the normal coordinate analysis for the actual determination of L coefficients. At absolute zero temperature

$$\delta_k(0) = \frac{h}{8\pi^2 c \omega_k} \qquad (2.22)$$

and $$\sum_{ij}(0) = \sum_k \frac{h}{8\pi^2 c \omega_k} L_{ik} L_{ij} \qquad (2.23)$$

The corresponding mean-square amplitudes of vibration will be found on the main diagonal of the $\sum$ matrix.

THERMODYNAMIC PARAMETERS

For calculating the thermodynamic parameters the molecules are assumed to be free. The rigid-rotor and harmonic approximations are assumed to be valid for rotations and vibrations respectively. The expressions used for calculation of thermodynamic quantities[6] are as follows:

Heat Capacity

$$C_p^\circ = 4R + \left(\frac{hc}{kT}\right)^2 R \sum_i \frac{d_i \, w_i \exp(-w_i \, hc/kT)}{\left[1 - \exp(-w_i \, hc/kT)\right]^2} \qquad (2.24)$$

Heat Content

$$\frac{H^\circ - E_o^\circ}{T} = 4R + R\left(\frac{hc}{kT}\right) \sum_i \frac{d_i \, w_i \exp(-w_i hc/kT)}{1 - \exp(-w_i hc/kT)} \qquad (2.25)$$

Entropy

$$S^\circ = \text{Entropy (v)} + \text{Entropy (Tr)} + \text{Entropy (Ro)} \qquad (2.26)$$

$$\text{Entropy (v)} = R \sum_i d_i \log_e \left[1 - \exp(-w_i hc/kT)\right] + R\left(\frac{hc}{kT}\right) x \sum_i \frac{d_i \, w_i \exp(-w_i \, hc/kT)}{1 - \exp(-w_i \, hc/kT)} \qquad (2.27)$$

$$\text{Entropy (Tr)} = 2.2868\left[5\log_{10}(T) + 3\log_{10}(M)\right] - 2.3135 \quad .. (2.28)$$

$$\text{Entropy (Ro)} = 2.2868\left[3\log_{10}(T) + 3\log_{10}(A\ B\ C) - 2\log_{10}(\sigma)\right] - 5.3838 \quad .. (2.29)$$

Free Energy

$$\frac{F^{o}-E^{o}_{o}}{T} = \text{Entropy(Tr)} + \text{Entropy (Ro)} - \sum_{i} d_i \log_e\left[1-\exp(-w_i\ hc/kT)\right] - 7.9452 \quad (2.30)$$

Summations are over all the vibrational frequencies, d_i is the degeneracy of the vibrational mode. E^{o}_{o} is the zero point energy. The notations used in above expressions are given below:

T = Temperature in Absolute scale

w_i = i^{th} Vibrational frequency

d_i = Degeneracy of the i^{th} mode

W = Molecular weight

σ = Symmetry Number ($\sigma = 6$ for D_{3h} point group)

A, B, C = Moment of inertia in atomic mass units and angstrom units.

Entropy(v) = Entropy of the molecule due to vibrations

Entropy (Tr) = Entropy of the molecule due to Translation

Entropy (Ro) = Entropy of the molecule due to Rotations

R = Gas constant

h = Plank's constant

c = Velocity of light.

THE USE OF NEUTRON SCATTERING

The technique of inelastic neutron scattering has been applied to study the low lying vibrations in molecular systems[7-10]. The usefulness of this technique arises from the fact that the energy of the thermal neutron is of the order of low frequency vibrational and lattice modes and their wavelength is comparable to that of the atomic spacing. This results in energy and momentum transfer of the thermal neutrons to be readily observed. Since neutron scattering involves short-range neutron-nucleus interactions in contrast to the electromagnetic interactions in infrared absorption and Raman scattering, the resulting intensity does not depend on the changes in electric dipole moment and polarizability. Because of the symmetry dependent selection rules, only a part of the information regarding molecular dynamics can be obtained from infrared absorption and Raman scattering, whereas neutron scattering being free from such constraints provides additional information about molecular systems.

Experimental Technique

The neutron scattering experiments have been obtained from a time-of-flight spectrometer details of which are available elsewhere[8]. A short description of the spectrometer is given here. A quasi-monochromatic beam of neutrons with a cut-off in thermal energy region is obtained by passing through a polycrystalline Beryllium sample. Neutrons

scattered by the sample S in the direction at right angles with respect to incident beam are chopped into brusts by a rotating collimator. The chopper thus provides a reference time at which the neutrons initiate their flight to the detector. Their velocity and hence energy distribution is determined by measuring their flight time over a 5-meter path between chopper and detector. Figure 1 shows the schematic drawing of the time-of-flight spectrometer.

Theory

The scattering of neutrons can be coherent or incoherent phenomena depending upon the orientation of nuclear spin and isotopic effects. The scattering of neutron wave from a system of identical nuclei of zero spin would be, except for magnetic interations with atomic electrons, entirely coherent and interference among the scattered waves is possible. For a system of identical nuclei with nonzero spin, the neutron-nuclear interaction depends on the relative orientation of neutrons and nuclear spins which gives rise to incoherence. In this case, each nucleus scatters independently. For nuclei with zero spin, incoherence can persist if the scattering length fluctuates from nucleus to nucleus because of isotopic effects. Coherent and incoherent scattering together allow a complete investigation of the structure and dynamics of the scatterer. For example, elastic coherent neutron scattering is used for structural investigations and inelastic coherent

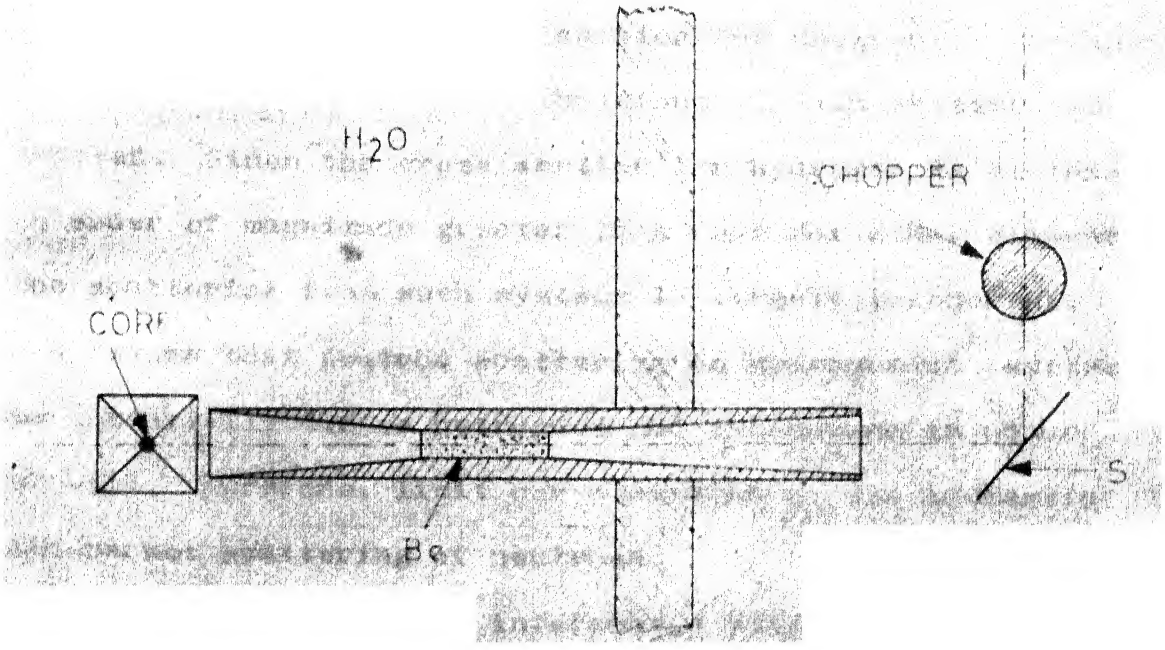

FIG. 1 : SCHEMATIC OF A COLD NEUTRON FACILITY

neutron scattering can be used for the determination of dispersion relations for oriented single crystals. On the other hand, incoherent (elastic and inelastic) neutron scattering can be used for studying the dynamics of the atomic system. Several molecular systems contain appreciable amount of hydrogen atoms which gives rise to a very large incoherent scattering cross section for neutrons. Considerable information for molecular vibrations of such systems can be derived. Since the cross section for hydrogen is at least an order of magnitude greater than that for other elements, the scattering from such systems is largely incoherent. We can assume that neutron scattering in hydrogenous systems is essentially due to hydrogens and incoherent in nature. We will, therefore, limit our attention to the inelastic incoherent scattering of neutrons.

The fact that the interaction between the neutrons and the phonons is of short-range and weak, allows the use of the Fermi pseudo-potential.

$$U(\bar{r}, \bar{R}_1, \ldots, \bar{R}_N) = \frac{2\pi\hbar^2}{m} \sum_{l=1}^{N} a_l \, \delta(\bar{r} - \bar{R}_l) \qquad (2.31)$$

where m is the neutron mass, $\bar{r}$ and $\bar{R}$ are neutron and nuclear position vectors and the scatterer is a system of N nuclei each labelled by subscript 'l'. The Fermi pseudo-potential contains as a parameter the bound nucleus scattering length 'a'. This is a measure of the strength

of the interaction. For a scattering system of identical nuclei having zero spin, 'a' is simply a constant. If the scatterer is an isotopic mixture or if the nuclei have non-zero spin, the scattering length has to be modified to take into account the spin dependence of the interaction. The effect arises because of the interactions in which neutron and nuclear spins are parallel, are different from those in which the spins are antiparallel. The total interaction in terms of the neutron and nuclear spin operators is then taken to be

$$U(\bar{r}, \bar{R}_1, \ldots, \bar{R}_N) = \frac{2\pi\hbar^2}{m} \sum_l \left[a_l + b_l(\bar{s}\cdot\bar{I}_l) \right] \delta(\bar{r} - \bar{R}_l) \quad .. (2.32)$$

where b_l is the spin dependent scattering length l and $\bar{I}_l$ are the neutron and nuclear spin operators.

The scattering probability can be separated into a factor depending on the initial and final neutron energy and a 'scattering law', which depends only on the molecular dynamics of the scattering system. The expression on which the theory is based is given by

$$\frac{d^2\sigma}{d\Omega dE_f} = \left(\frac{E_f}{E_o}\right)^{\frac{1}{2}} N \left[a^2_{coh} S_c(\bar{k},\omega) + a^2_{inc} S_i(\bar{k},\omega) \right] \quad .. (2.33)$$

Here $\frac{d^2\sigma}{d\Omega dE_f}$ is the differential scattering cross-section per unit solid angle and per unit final neutron energy, for a neutron of momentum $\bar{k}_i$ to scatter with momentum transfer

$$\bar{K} = \bar{k}_i - \bar{k}_f \qquad (2.34)$$

and energy transfer

$$\hbar\omega = E_i - E_f = \hbar^2 (k_i^2 - k_f^2)/2m \qquad (2.35)$$

S_c and S_i are the scattering laws for coherent and incoherent scattering respectively. The above expression (equation (2.33)) is for scattering from a system of N atoms which are identical except for a completely disordered distribution of nuclear spins and isotopic species. The generalization to molecules with different atoms is straightforward. As mentioned earlier, the neutron spectra of materials containing hydrogen, the most intense lines correspond to vibrations involving hydrogenous units and normally only the incoherent contribution from hydrogen is considered in analysing such spectra.

For a general lattice, the differential scattering cross-section for incoherent scattering can be written as a series of terms giving the probability of absorption or emission of zero, one, or several phonons.

$$\frac{d^2\sigma_{inc}}{d\Omega dE_f} = \sum_1 \frac{d^2\sigma_{inc}^{(1)}}{d\Omega dE_f} \qquad (2.36)$$

where 1 is the number of phonons involved in the interaction. The largest contribution to scattering is from the single-phonon (1=1) term with successive terms diminishing in magnitude. At low temperature, the main contribution

to the total incoherent scattering comes only from this "one-phonon" interaction and in practical calculations, higher order terms are neglected. This one-phonon approximation contains the assumption that the vibrations of atoms about their equilibrium positions in the lattice are harmonic and that phonon energies $\hbar\omega$ are greater than $k_B T$.

In the one-phonon approximation, the incoherent scattering cross-section for a polycrystalline sample can be written as:

$$\frac{d^2\sigma_{inc}}{d\Omega\, dE_f} = \left(\frac{E_f}{E_i}\right)^{\frac{1}{2}} \frac{\left[E_i + E_f - 2(E_i E_f)^{\frac{1}{2}} \cos\phi\right]}{\omega \exp\left(\hbar\omega/k_B T - 1\right)} \sum a_{l_{inc}}^2 \exp\left(-2W_l\right) g_l''(\omega) \quad .. (2.37)$$

where ϕ is the scattering angle, $a_{l_{inc}}$ is the incoherent scattering length of the l^{th} nucleus in the unit cell, $\exp(-2W_l)$ is the Debye-Waller factor for the l^{th} nucleus and the sum over l includes all the n atoms in a unit cell. Here

$$g_l''(\omega) = \frac{m}{M_l} \frac{V}{(2\pi)^3} \frac{1}{3} \sum_j \int d^3q\, \bar{C}_j^l(\bar{q})^2\, \delta\left(\omega - \omega_j(\bar{q})\right) \quad (2.38)$$

where M_l is the mass of the l^{th} nucleus, m is the neutron mass, V is the unit cell volume, $\bar{q}$ is the phonon wave-vector. The index j takes on $3n$ values corresponding to $3n$ branches of the dispersion relation. $\bar{C}_j^l(\bar{q})$ are the polarization vectors mentioned previously.

In the case of monoatomic polycrystalline sample, the sum over 1 reduces to

$$\sum_{1} a_{1_{inc}}^{2} \exp(-2W_1)\, g_1''(\omega) = a_{inc}^{2} \exp(-2W)\, \frac{m}{M'}\, g''(\omega) \quad (2.39)$$

where a_{inc} is the incoherent scattering length, M' is the mass of the atom and $g''(\omega)$ is the effective frequency distribution, defined as in equation (2.38) above. The true phonon frequency distribution may be formally defined as

$$g(\omega) = \frac{V}{(2\pi)^3}\, \frac{1}{3} \sum_{j} \int d^3q\; \delta\left(\omega - \omega_j(\bar{q})\right) \quad (2.40)$$

Although $g(\omega)$ and $g''(\omega)$ are not directly related, comparison of equations (2.38) and (2.40) shows that the true phonon frequency distribution has to be weighted by the square of the polarization vectors before it can be compared with the frequency distributions obtained from measurements of neutron scattering cross-sections.

Although the frequency distributions obtained from equation (2.37) involve the use of several approximations, they do provide useful information and are found to be in qualitative, if not quantitative, agreement with calculated distributions. While relative intensities of the contributions of the individual modes to $g(\omega)$ and shape of the individual peaks may be inexact, the frequencies of the modes can be obtained and identified. It should be noted that the cases where only the normal modes of vibrations

are obtained (not the dispersion relations) assuming the molecules to be free, equations (2.38) and (2.40) can be approximately calculated without the integration over the phonon wave-vector ($\bar{q}$). Relative intensity of the peaks in neutron spectrum helps in assignments of peak positions. The neutron spectrum of 1,3,5-triamino-2,4,6-trinitrobenzene (TATNB) has been obtained and discussed in the next chapter.

Infrared and Raman techniques used for the vibration spectra of TATNB (Chapter III) are very well developed[2,11,12] and are not discussed here.

REFERENCES

1. E.B. Wilson, Jr., J. Chem. Phys. 7, 1047 (1939); 9, 76 (1941).

2. E.B. Wilson, Jr., J.C. Decius and P.C. Cross, "Molecular Vibrations", McGraw-Hill, New York (1955).

3. J. Overend and J.R. Scherer, J. Chem. Phys. 32, 1289 (1960).

4. Y. Morino and K. Kuchitsu, J. Chem. Phys. 20, 1809 (1953); I. Nakagawa, J. Chem. Soc. Japan 74, 243 (1953).

5. S.J. Syvin, "Molecular Vibrations and Mean Square Amplitudes", Elsevier, Amsterdam (1968), p. 89-100.

6. G. Herzberg, "Infrared and Raman Spectra of Polyatomic Molecules", Van Nostrand, Princeton (1945).

7. T. Miyazava and E.R. Blout, J. Am. Chem. Soc. 83, 712 (1961).

8. H. Boutin and S. Yip, "Molecular Spectroscopy with Neutrons", M.I.T. Press, Cambridge (1968).

9. A.P. Egelstaff, "Thermal Neutron Scattering", Academic Press, New York (1965), Chapter 10.

10. L.S. Kothari and K.S. Singwi, Solid State Physics 8, 109 (1959).

11. H.A. Szymanski, "Raman Spectroscopy", Plenum Press, New York (1967).

12. K. Nakanishi, "Infrared Absorption Spectroscopy", Holden-Day, San Francisco (1962).

CHAPTER - III

VIBRATION SPECTRA OF

1,3,5-TRIAMINO-2,4,6-TRINITROBENZENE

1,3,5-Triamino-2,4,6-trinitrobenzene (TATNB) is unusual in its thermal and solubility behaviour. It decomposes above 300°C and dissolves best in concentrated sulphuric acid only. Its structure has been recently reported by Cady and Larson[1]. The unit cell is triclinic with the space group $P\bar{1}$ and cell dimensions a = 9.01 Å, b = 9.028 Å, c = 6.812 Å, and α = 108.59°, β = 91.82°, γ = 119.97°. There are two molecules per cell. It is found that the aromatic carbon-carbon distance is 1.441 Å, the carbon-amino nitrogen distance is 1.316 Å and there are six bifurcated nitrogen-oxygen hydrogen bonds. The hydrogen bonding is similar to the compound 1,3-diamino-2,4,6-trinitrobenzene[2]. The optical and cleavage properties of the crystal indicate that the molecules are arranged in planar sheets parallel to the a-b plane. This is confirmed by X-ray structure determination. The planar sheet structure greatly simplifies the calculation of normal vibrations of the system. The structure of the TATNB molecule is shown in Figure 2. Special interest in the molecule is because of the simultaneous substitution of electron donor and acceptor groups.

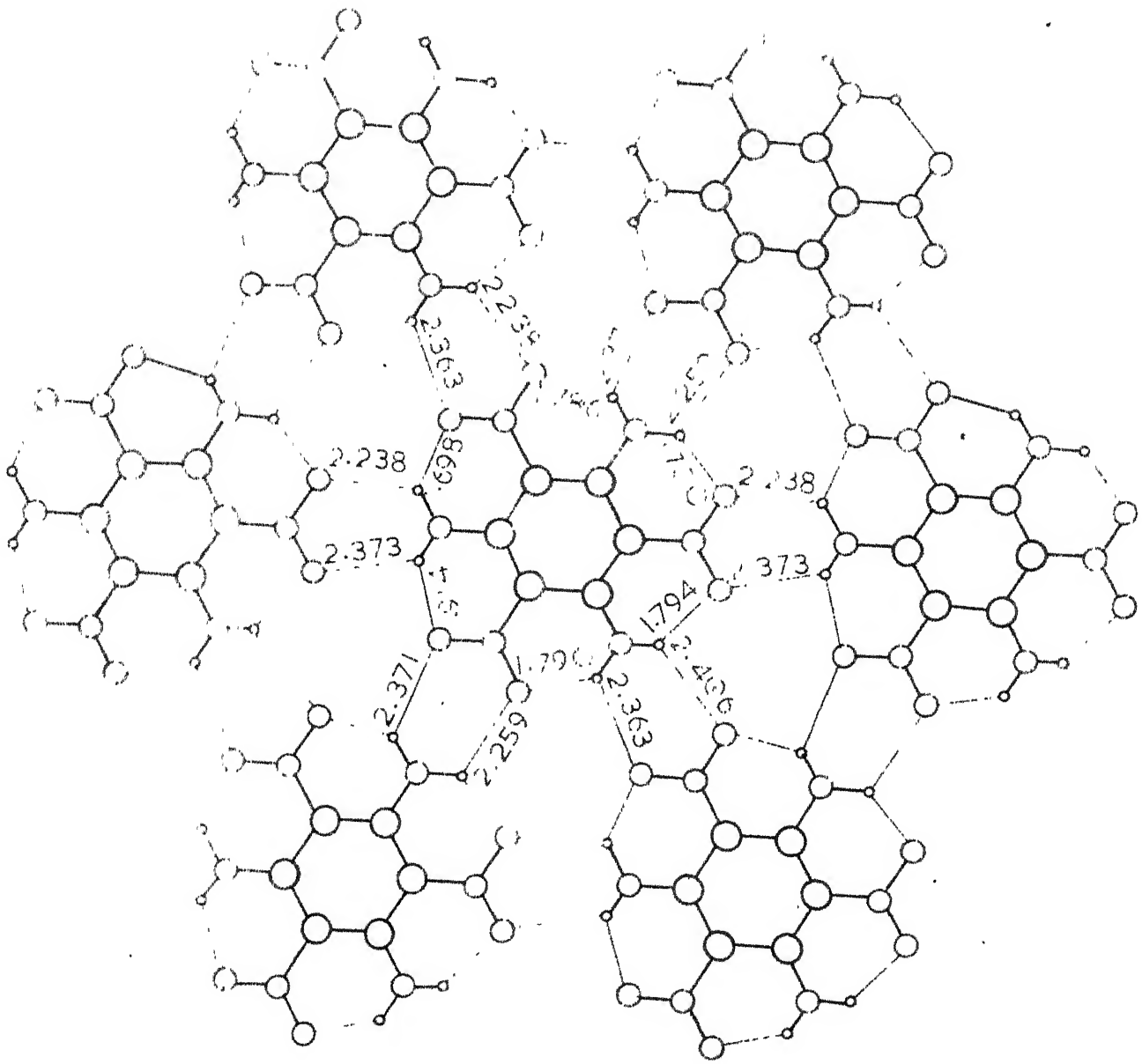

Fig 2 Structure of TATNB showing inter and intra molecular hydrogen bond distances

GROUP THEORETICAL ANALYSIS

The molecule belongs to D_{3h} point group symmetry. There are 24 atoms in the molecule and 66 (24 x 3 - 6) fundamental modes of vibration. The number of normal modes belonging to different symmetry species have been calculated using the relation (2.10). Character Table, optical activity and number of fundamental modes for each symmetry species are given in Table 1.

CALCULATIONS OF NORMAL VIBRATIONS

A complete vibrational analysis has been carried out using Wilson GF matrix method[3]. The coordinates of the atoms are based on the average bond lengths:

$$\ell(C\text{–}N)_O = 1.422\ \text{Å}, \quad \ell(C\text{–}N)_H = 1.316\ \text{Å},$$
$$\ell(C\text{–}C) = 1.441\ \text{Å}, \quad \ell(N\text{–}O) = 1.242\ \text{Å},$$
$$\ell(N\text{–}H) = 0.925\ \text{Å}.$$

All the angles between bonds are taken to be 120°. The internal coordinates used in these calculations are as follows:

Bond stretching :

$$r(C\text{–}N)_O,\ r(N\text{–}O),\ r(C\text{–}C),\ r(C\text{–}N)_H,\ r(N\text{–}H).$$

In-plane angle bending :

$$\phi(C\text{–}C\text{–}C)_O,\ \phi(C\text{–}C\text{–}N)_O,\ \phi(C\text{–}N\text{–}O),\ \phi(O\text{–}N\text{–}O),\ \phi(C\text{–}C\text{–}C)_H,$$
$$\phi(C\text{–}C\text{–}N)_H,\ \phi(C\text{–}N\text{–}H),\ \phi(H\text{–}N\text{–}H).$$

Out-of-plane wagging :

$$\omega(C\text{–}NO_2),\ \omega(C\text{–}NH_2),\ \omega(R\text{–}N)_O,\ \omega(R\text{–}N)_H.$$

TABLE 1

CHARACTER TABLE, NUMBER OF NORMAL MODES FOR EACH SYMMETRY SPECIES AND OPTICAL ACTIVITY FOR D_{3h} SYMMETRY POINT GROUP

	E	$2C_3$	$3C_2$	σ_h	$2S_3$	$3\sigma_v$	N[a]	Optical activity
A_1'	1	1	1	1	1	1	8	Raman
A_2'	1	1	-1	1	1	-1	7	
E'	2	-1	0	2	-1	0	30	Raman, I.R.
A_1''	1	1	1	-1	-1	-1	2	
A_2''	1	1	-1	-1	-1	1	5	I.R.
E''	2	-1	0	-2	1	0	14	Raman

[a] 'N' is the number of normal modes in the species.

Torsional coordinates :

$$t(C-C), \quad t(C-N)_O, \quad t(C-N)_H$$

The out-of-plane modes include six benzene skeleton torsions and six torsions round (C—N) bonds. (C—C) torsion is sum of torsions due to (C—C) bonds and (C—N) bonds (sum of two torsions) whereas (C—N) torsion is sum of all four possible torsions, the resulting force constants should be accordingly interpreted. Using these definitions of internal coordinates G matrix is calculated and shown in Table 2. Symmetry coordinates have been written down as a normalized linear combination of internal coordinates. The definition of internal coordinates, and corresponding symmetry coordinates are given in Appendix. Symmetry coordinates were used in construction of U-matrix which factors the G-matrix in a block diagonal structure.

Urey-Bradley force field is used for the potential energy matrix. The expression for such a potential function for the molecule is given by[4]

$$V = \sum_{j,k} K'_{jk}\, r_{jk}(\triangle r_{jk}) + \frac{1}{2} K_{jk} (\triangle r_{jk})^2$$

$$+ \sum_{i,j,k} H'_{ijk}\, r_{ij}\, r_{jk} (\triangle \phi_{ijk}) + \frac{1}{2} H_{ijk}\, r_{ij}\, r_{jk} (\triangle \phi_{ijk})^2$$

$$+ \sum_{i,j,k} F'_{ik}\, q_{ik} (\triangle q_{ik}) + \frac{1}{2} F_{ik} (\triangle q_{ik})^2$$

$$+ \sum_{j} K^{t}_{j} (\triangle t_j)^2 + \sum_{j} K^{\omega}_{j} (\triangle \omega_j)^2$$

TABLE 2

G MATRIX ELEMENTS FOR TATNB*

I	J	G(I,J)	I	J	G(I,J)	I	J	G(I,J)	I	J	G(I,J)
1	1	0.155	1	2	-0.036	1	3	-0.036	1	4	-0.042
1	24	-0.042	1	25	0.100	1	26	-0.050	1	27	-0.050
1	28	-0.050	1	29	0.100	1	30	-0.050	1	31	-0.050
1	33	0.050	1	55	-0.050	1	56	0.050	2	2	0.134
2	3	-0.036	2	26	-0.043	2	27	0.043	2	28	0.093
2	29	-0.050	2	30	-0.043	3	3	0.134	3	26	0.043
3	27	-0.043	3	28	-0.043	3	29	-0.050	3	30	0.093
4	4	0.167	4	5	-0.042	4	8	-0.042	4	24	-0.042
4	25	-0.050	4	26	-0.051	4	27	0.101	4	28	0.051
4	30	-0.051	4	31	-0.050	4	32	0.105	4	33	-0.055
4	34	-0.055	4	36	0.055	4	37	0.050	4	39	-0.050
4	55	0.050	4	56	-0.050	5	5	0.155	5	6	-0.036
5	7	-0.036	5	8	-0.042	5	25	-0.050	5	26	0.050
5	31	0.100	5	32	-0.050	5	33	-0.050	5	34	-0.067
5	35	0.134	5	36	-0.067	5	37	-0.050	5	39	0.050
6	6	1.063	6	7	-0.036	6	32	-0.047	6	33	0.047
6	34	0.114	6	35	-0.067	6	36	-0.047	7	7	1.063
7	32	0.047	7	33	-0.047	7	34	-0.047	7	35	-0.067
7	36	0.114	8	8	0.167	8	9	-0.042	8	12	-0.042
8	25	0.050	8	26	-0.050	8	31	-0.050	8	32	-0.055
8	33	0.105	8	34	0.055	8	36	-0.055	8	37	-0.050
8	38	0.101	8	39	-0.051	8	40	-0.051	8	42	0.051
8	43	0.050	8	45	-0.050	9	9	0.155	9	10	-0.036
9	11	-0.036	9	12	-0.042	9	31	-0.050	9	32	0.050
9	37	0.100	9	38	-0.050	9	39	-0.050	9	40	-0.050
9	41	0.100	9	42	-0.050	9	43	-0.050	9	45	0.050
10	10	0.134	10	11	-0.036	10	38	-0.043	10	39	0.043

.. Contd.

*See footnote at the end of the table.

Table 2 (contd.)

I	J	G(I,J)	I	J	G(I,J)	I	J	G(I,J)	I	J	G(I,J)
10	40	0.093	10	41	-0.050	10	42	-0.043	11	11	0.134
11	38	0.043	11	39	-0.043	11	40	-0.043	11	41	-0.050
11	42	0.093	12	12	0.167	12	13	-0.042	12	16	-0.042
12	31	0.050	12	32	-0.050	12	37	-0.050	12	38	-0.051
12	39	0.101	12	40	0.051	12	42	-0.051	12	43	-0.050
12	44	0.105	12	45	-0.055	12	46	-0.055	12	48	0.055
12	49	0.050	12	51	-0.050	13	13	0.155	13	14	-0.036
13	15	-0.036	13	16	-0.042	13	37	-0.050	13	38	0.050
13	43	0.100	13	44	-0.050	13	45	-0.050	13	46	-0.067
13	47	0.134	13	48	-0.067	13	49	-0.050	13	51	0.050
14	14	1.063	14	15	-0.036	14	44	-0.047	14	45	0.047
14	46	0.114	14	47	-0.067	14	48	-0.047	15	15	1.063
15	44	0.047	15	45	-0.047	15	46	-0.047	15	47	-0.067
15	48	0.114	16	16	0.167	16	17	-0.042	16	20	-0.042
16	37	0.050	16	38	-0.050	16	43	-0.050	16	44	-0.055
16	45	0.105	16	46	0.055	16	48	-0.055	16	49	-0.050
16	50	0.101	16	51	-0.051	16	52	-0.051	16	54	0.051
16	55	0.050	16	57	-0.050	17	17	0.155	17	18	-0.036
17	19	-0.036	17	20	-0.042	17	43	-0.050	17	44	0.050
17	49	0.100	17	50	-0.050	17	51	-0.050	17	52	-0.050
17	53	0.100	17	54	-0.050	17	55	-0.050	17	57	0.050
18	18	0.134	18	19	-0.036	18	50	-0.043	18	51	0.043
18	52	0.093	18	53	-0.050	18	54	-0.043	19	19	0.134
19	50	0.043	19	51	-0.043	19	52	-0.043	19	53	-0.050
19	54	0.093	20	20	0.167	20	21	-0.042	20	24	-0.042
20	25	0.050	20	27	-0.050	20	43	0.050	20	44	-0.050
20	49	-0.050	20	50	-0.051	20	51	0.101	20	52	0.051
20	54	-0.051	20	55	-0.050	20	56	0.105	20	57	-0.055
20	58	-0.055	20	60	0.055	21	21	0.155	21	22	-0.036

.. Contd.

Table 2 (contd.)

I	J	G(I,J)	I	J	G(I,J)	I	J	G(I,J)	I	J	G(I,J)
21	23	-0.036	21	24	-0.042	21	25	-0.050	21	27	0.050
21	49	-0.050	21	50	0.050	21	55	0.100	21	56	-0.050
21	57	-0.050	21	58	-0.067	21	59	0.134	21	60	-0.067
22	22	1.063	22	23	-0.036	22	56	-0.047	22	57	0.047
22	58	0.114	22	59	-0.067	22	60	-0.047	23	23	1.063
23	56	0.047	23	57	-0.047	23	58	-0.047	23	59	-0.067
23	60	0.114	24	24	0.167	24	25	-0.050	24	26	0.101
24	27	-0.051	24	28	-0.051	24	30	0.051	24	31	0.050
24	33	-0.050	24	49	0.050	24	50	-0.050	24	55	-0.050
24	56	-0.055	24	57	0.105	24	58	0.055	24	60	-0.055
25	25	0.201	25	26	-0.100	25	27	-0.100	25	31	-0.120
25	32	-0.002	25	33	0.122	25	34	0.022	25	36	-0.022
25	37	0.020	25	39	-0.020	25	49	0.020	25	50	-0.020
25	55	-0.120	25	56	0.122	25	57	-0.002	25	58	-0.022
25	60	0.022	26	26	0.197	26	27	-0.097	26	28	-0.117
26	30	0.117	26	31	0.121	26	32	0.002	26	33	-0.123
26	34	-0.022	26	36	0.022	26	37	-0.020	26	39	0.020
27	27	0.197	27	28	0.117	27	30	-0.117	27	49	-0.020
27	50	0.020	27	55	0.121	27	56	-0.123	27	57	0.002
27	58	0.022	27	60	-0.022	28	28	0.204	28	29	-0.110
28	30	-0.094	28	31	-0.020	28	33	0.020	28	55	0.020
28	56	-0.020	29	29	0.220	29	30	-0.110	30	30	0.204
30	31	0.020	30	33	-0.020	30	55	-0.020	30	56	0.020
31	31	0.201	31	32	-0.100	31	33	-0.100	31	37	-0.120
31	39	0.121	31	40	0.020	31	42	-0.020	31	43	0.020
31	45	-0.020	31	55	0.020	31	56	-0.020	32	32	0.213
32	33	-0.113	32	34	-0.141	32	36	0.141	32	37	0.122
32	39	-0.123	32	40	-0.020	32	42	0.020	32	43	-0.020

.. Contd.

Table 2 (contd.)

I	J	G(I,J)	I	J	G(I,J)	I	J	G(I,J)	I	J	G(I,J)
32	45	0.020	33	33	0.213	33	34	0.141	33	36	-0.141
33	37	-0.002	33	39	0.002	33	55	-0.020	33	56	0.020
34	34	1.391	34	35	-1.285	34	36	-0.106	34	37	-0.022
34	39	0.022	35	35	2.569	35	36	-1.285	36	36	1.391
36	37	0.022	36	39	-0.022	37	37	0.201	37	38	-0.100
37	39	-0.100	37	43	-0.120	37	44	-0.002	37	45	0.122
37	46	0.022	37	48	-0.022	37	49	0.020	37	51	-0.020
38	38	0.197	38	39	-0.097	38	40	-0.117	38	42	0.117
38	43	0.121	38	44	0.002	38	45	-0.123	38	46	-0.022
38	48	0.022	38	49	-0.020	38	51	0.020	39	39	0.197
39	40	0.117	39	42	-0.117	39	43	-0.000	40	40	0.204
40	41	-0.110	40	42	-0.094	40	43	-0.020	40	45	0.020
41	41	0.220	41	42	-0.110	42	42	0.204	42	43	0.020
42	45	-0.020	43	43	0.201	43	44	-0.100	43	45	-0.100
43	49	-0.120	43	50	-0.000	43	51	0.121	43	52	0.020
43	54	-0.020	43	55	0.020	43	57	-0.020	44	44	0.213
44	45	-0.113	44	46	-0.141	44	48	0.141	44	49	0.122
44	51	-0.123	44	52	-0.020	44	54	0.020	44	55	-0.020
44	57	0.020	45	45	0.213	45	46	0.141	45	48	-0.141
45	49	-0.002	45	51	0.002	46	46	1.391	46	47	-1.285
46	48	-0.106	46	49	-0.022	46	51	0.022	47	47	2.569
47	48	-1.285	48	48	1.391	48	49	0.022	48	51	-0.022
49	49	0.201	49	50	-0.100	49	51	-0.100	49	55	-0.120
49	56	-0.002	49	57	0.122	49	58	0.022	49	60	-0.022
50	50	0.197	50	51	-0.097	50	52	-0.117	50	54	0.117
50	55	0.121	50	56	0.002	50	57	-0.123	50	58	-0.022
50	60	0.022	51	51	0.197	51	52	0.117	51	54	-0.117
52	52	0.204	52	53	-0.110	52	54	-0.094	52	55	-0.020
52	57	0.020	53	53	0.220	53	54	-0.110	54	54	0.204

.. Contd.

Table 2 (contd.)

I	J	G(I,J)	I	J	G(I,J)	I	J	G(I,J)	I	J	G(I,J)
54	55	0.020	54	57	-0.020	55	55	0.201	55	56	-0.100
55	57	-0.100	56	56	0.213	56	57	-0.113	56	58	-0.141
56	60	0.141	57	57	0.213	57	58	0.141	57	60	-0.141
58	58	1.391	58	59	-1.285	58	60	-0.106	59	59	2.569
59	60	-1.285	60	60	1.391	61	61	0.504	61	67	0.239
61	68	-0.041	61	72	-0.041	61	73	-0.135	61	74	-0.047
61	77	0.047	61	78	0.135	61	80	0.094	61	84	-0.094
62	62	2.977	62	67	-0.044	62	68	0.294	62	69	-0.044
62	73	0.188	62	74	-0.188	62	75	-0.051	62	78	0.051
62	79	-0.101	62	81	0.101	63	63	0.504	63	68	-0.041
63	69	0.239	63	70	-0.041	63	73	0.047	63	74	0.135
63	75	-0.135	63	76	-0.047	63	80	-0.094	63	82	0.094
64	64	2.977	64	69	-0.044	64	70	0.294	64	71	-0.044
64	74	0.051	64	75	0.188	64	76	-0.188	64	77	-0.051
64	81	-0.101	64	83	0.101	65	65	0.504	65	70	-0.041
65	71	0.239	65	72	-0.041	65	75	0.047	65	76	0.135
65	77	-0.135	65	78	-0.047	65	82	-0.094	65	84	0.094
66	66	2.977	66	67	-0.044	66	71	-0.044	66	72	0.294
66	73	-0.051	66	76	0.051	66	77	0.188	66	78	-0.188
66	79	0.101	66	83	-0.101	67	67	0.480	67	68	-0.245
67	69	0.040	67	71	0.040	67	72	-0.245	67	73	-0.001
67	74	-0.135	67	75	0.046	67	76	-0.046	67	77	0.135
67	78	0.001	67	80	0.279	67	81	-0.093	67	83	0.093
67	84	-0.279	68	68	0.506	68	69	-0.245	68	70	0.040
68	72	0.040	68	73	0.015	68	74	-0.015	68	75	-0.143
68	76	0.046	68	77	-0.046	68	78	0.143	68	79	-0.287
68	81	0.287	68	82	-0.093	68	84	0.093	69	69	0.480
69	70	-0.245	69	71	0.040	69	73	0.135	69	74	0.001
69	75	-0.001	69	76	-0.135	69	77	0.046	69	78	-0.046

.. Contd.

Table 2 (contd.)

I	J	G(I,J)	I	J	G(I,J)	I	J	G(I,J)	I	J	G(I,J)
69	79	0.093	69	80	-0.279	69	82	0.279	69	83	-0.093
70	70	0.506	70	71	-0.245	70	72	0.040	70	73	-0.046
70	74	0.143	70	75	0.015	70	76	-0.015	70	77	-0.143
70	78	0.046	70	80	0.093	70	81	-0.287	70	83	0.287
70	84	-0.093	71	71	0.480	71	72	-0.245	71	73	0.046
71	74	-0.046	71	75	0.135	71	76	0.001	71	77	-0.001
71	78	-0.135	71	79	-0.093	71	81	0.093	71	82	-0.279
71	84	0.279	72	72	0.506	72	73	-0.143	72	74	0.046
72	75	-0.046	72	76	0.143	72	77	0.015	72	78	-0.015
72	79	0.287	72	80	-0.093	72	82	0.093	72	83	-0.287
73	73	0.210	73	74	-0.054	73	75	-0.006	73	76	-0.107
73	77	-0.006	73	78	-0.037	73	79	-0.117	73	80	-0.108
73	81	0.010	73	82	0.107	73	83	0.107	73	84	0.001
74	74	0.210	74	75	-0.037	74	76	-0.006	74	77	-0.107
74	78	-0.006	74	79	0.010	74	80	-0.108	74	81	-0.117
74	82	0.001	74	83	0.107	74	84	0.107	75	75	0.210
75	76	-0.054	75	77	-0.006	75	78	-0.107	75	79	0.107
75	80	0.001	75	81	-0.117	75	82	-0.108	75	83	0.010
75	84	0.107	76	76	0.210	76	77	-0.037	76	78	-0.006
76	79	0.107	76	80	0.107	76	81	0.010	76	82	-0.108
76	83	-0.117	76	84	0.001	77	77	0.210	77	78	-0.054
77	79	0.010	77	80	0.107	77	81	0.107	77	82	0.001
77	83	-0.117	77	84	-0.108	78	78	0.210	78	79	-0.117
78	80	0.001	78	81	0.107	78	82	0.107	78	83	0.010
78	84	-0.108	79	79	0.860	79	81	-0.214	79	83	-0.214
80	80	12.795	80	82	-0.214	80	84	-0.214	81	81	0.860
81	83	-0.214	82	82	12.795	82	84	-0.214	83	83	0.860
84	84	12.795									

*Only nonzero elements are listed. The numbering of the internal coordinates is in accordance with the order in which they are listed in the text. G matrix is symmetric, only elements on the main diagonal and above it are listed

where $\triangle r_{jk}$, $\triangle \phi_{ijk}$, $\triangle t_j$, $\triangle \omega_j$ are the internal coordinates corresponding to bond stretch, angle-bend, torsion and out-of-plane deformation respectively. The subscripts on the first two internal coordinates label the atoms involved. $\triangle t_j$ denotes the torsion about j^{th} bond and $\triangle \omega_j$ denotes the j^{th} bond out-of-plane wag from the benzene-ring plane. $\triangle q_{ik}$ are the changes in the nonbounded distances (one-three atom distances are taken for the purpose). The primed quantities are introduced as internal tensions and are taken as 1/10 of the valence force constants. The Z - matrix defined by equation (2.5) was first constructed for TATNB. The F-matrix is calculated from Z-matrix and a set of initial force constants. These force constants were assumed, based on simpler molecules and they were then modified to get an agreement of the calculated frequencies with observed infrared, Raman and neutron frequencies. Force constants which give best fit are given in Table 3 and the corresponding F-matrix is shown in Table 4.

The problem of transferability of force constants has been discussed in great detail by Scherer[5,6]. It is observed that the Urey-Bradley force field can be successfully transferred in some carbonyl, halogen containing molecules and in s-trihalogen substituted benzenes[7]. Similar successes were met with transfer of force field from symmetrical perhaloethylenes to mixed chlorofluoroethylenes[8].

TABLE 3

FORCE CONSTANTS (mdyn./Å) FOR TATNB[a]

		$K^{\omega}(N - O)$	= 0.33
		$K^{\omega}(N - H)$	= 0.12
$K(C-N)_O$	= 1.98	$K^{\omega}(R^{b} - N)_O$	= 0.12
$K(N-O)$	= 6.58	$K^{\omega}(R - N)_H$	= 0.09
$K(C-C)$	= 3.86		
$K(C-N)_H$	= 2.69		
$K(N-H)$	= 5.87	$K^{t}(C - C)$	= 0.22
		$K^{t}(C - N)_O$	= 0.030
		$K^{t}(C - N)_H$	= 0.0023
$H(C-C-C)_O$	= 0.28	$F(C \cdot C \cdot C)_O$	= 0.30
$H(C-C-N)_O$	= 0.88	$F(C \cdot C \cdot N)_O$	= 0.17
$H(C-N-O)$	= 1.08	$F(C \cdot N \cdot O)$	= 0.23
$H(O-N-O)$	= 0.90	$F(O \cdot N \cdot O)$	= 0.41
$H(C-C-C)_H$	= 0.32	$F(C \cdot C \cdot C)_H$	= 0.31
$H(C-C-N)_H$	= 1.14	$F(C \cdot C \cdot N)_H$	= 0.39
$H(C-N-H)$	= 0.45	$F(C \cdot N \cdot H)$	= 0.09
$H(H-N-H)$	= 0.35	$F(H \cdot N \cdot H)$	= 0.022

[a] K stands for bond stretches, H for angle bends, K^{ω} for out-of-plane wags, K^{t} for torsions and F for nonbounded interactions.

[b] 'R' represents benzene ring.

TABLE 4

F-MATRIX ELEMENTS FOR TATNB*

I	J	F(I,J)	I	J	F(I,J)	I	J	F(I,J)	I	J	F(I,J)
1	1	2.575	1	2	0.178	1	3	0.178	1	4	0.132
1	24	0.132	1	26	0.094	1	27	0.094	1	28	0.124
1	30	0.124	2	2	7.035	2	3	0.318	2	29	0.199
2	30	0.113	3	3	7.035	3	28	0.113	3	29	0.199
4	4	4.718	4	5	0.302	4	8	0.240	4	24	0.232
4	25	0.168	4	26	0.095	4	31	0.174	4	33	0.215
5	5	3.382	5	6	0.069	5	7	0.069	5	8	0.302
5	32	0.203	5	33	0.203	5	34	0.042	5	36	0.042
6	6	5.941	6	7	0.017	6	35	0.008	6	36	0.033
7	7	5.941	7	34	0.033	7	35	0.008	8	8	4.718
8	9	0.132	8	12	0.232	8	31	0.174	8	32	0.215
8	37	0.168	8	39	0.095	9	9	2.575	9	10	0.178
9	11	0.178	9	12	0.132	9	38	0.094	9	39	0.094
9	40	0.124	9	42	0.124	10	10	7.035	10	11	0.318
10	41	0.199	10	42	0.113	11	11	7.035	11	40	0.113
11	41	0.199	12	12	4.718	12	13	0.302	12	16	0.240
12	37	0.168	12	38	0.095	12	43	0.174	12	45	0.215
13	13	3.382	13	14	0.069	13	15	0.069	13	16	0.302
13	44	0.203	13	45	0.203	13	46	0.042	13	48	0.042
14	14	5.941	14	15	0.017	14	47	0.008	14	48	0.033
15	15	5.941	15	46	0.033	15	47	0.008	16	16	4.718
16	17	0.132	16	20	0.232	16	43	0.174	16	44	0.215
16	49	0.168	16	51	0.095	17	17	2.575	17	18	0.178
17	19	0.178	17	20	0.132	17	50	0.094	17	51	0.094
17	52	0.124	17	54	0.124	18	18	7.035	18	19	0.318
18	53	0.199	18	54	0.113	19	19	7.035	19	52	0.113
19	53	0.199	20	20	4.718	20	21	0.302	20	24	0.240
20	49	0.168	20	50	0.095	20	55	0.174	20	57	0.215

.. Contd.

*See footnote at the end of the table.

Table 4 (contd.)

I	J	F(I,J)	I	J	F(I,J)	I	J	F(I,J)	I	J	F(I,J)
21	21	3.382	21	22	0.069	21	23	0.069	21	24	0.302
21	56	0.203	21	57	0.203	21	58	0.042	21	60	0.042
22	22	5.941	22	23	0.017	22	59	0.008	22	60	0.033
23	23	5.941	23	58	0.033	23	59	0.008	24	24	4.718
24	25	0.168	24	27	0.095	24	55	0.174	24	56	0.215
25	25	0.482	26	26	0.993	27	27	0.993	28	28	1.213
29	29	1.106	30	30	1.213	31	31	0.529	32	32	1.380
33	33	1.380	34	34	0.480	35	35	0.356	36	36	0.480
37	37	0.482	38	38	0.993	39	39	0.993	40	40	1.213
41	41	1.106	42	42	1.213	43	43	0.529	44	44	1.380
45	45	1.380	46	46	0.480	47	47	0.356	48	48	0.480
49	49	0.482	50	50	0.993	51	51	0.993	52	52	1.213
53	53	1.106	54	54	1.213	55	55	0.529	56	56	1.380
57	57	1.380	58	58	0.480	59	59	0.356	60	60	0.480
61	61	0.330	62	62	0.124	63	63	0.330	64	64	0.124
65	65	0.330	66	66	0.124	67	67	0.119	68	68	0.090
69	69	0.119	70	70	0.090	71	71	0.119	72	72	0.090
73	73	0.225	74	74	0.225	75	75	0.225	76	76	0.225
77	77	0.225	78	78	0.225	79	79	0.030	80	80	0.002
81	81	0.030	82	82	0.002	83	83	0.030	84	84	0.002

*Only nonzero elements are listed. The numbering of the internal coordinates is in accordance with the order in which they are listed in the text (p. 29). F matrix is symmetric, only elements on the main diagonal and above it are listed.

EXPERIMENTAL

The infrared spectrum of polycrystalline sample of TATNB in the form of KBr pellets were obtained using Perkin Elmer 521 spectrometer in the region 5000 - 250 cm^{-1} and is shown in Figures 3 and 4. Laser-excited Raman spectrum has been recorded on Coderg spectrophotometer and shown in Figure 5. The inelastic neutron spectrum of TATNB recorded at the AMMRC slow chopper is shown in Figure 6. This was also helpful in assignments of the frequencies. Since TATNB is insoluble in almost all the solvents it was not possible to get an infrared or Raman spectrum in solution form. This made deuteration impossible.

DISCUSSION

The calculated and observed frequencies in I.R., Raman and neutron scattering and their possible assignments based on potential energy distribution, symmetry principles, peak intensities, bond order and group frequencies are given in Table 5. The detailed discussion for assignments of the modes follows.

NH_2 Group Frequencies

The intense broad bands in infrared spectrum at 3328 and 3227 cm^{-1} are assigned to NH_2 asymmetric and symmetric stretches respectively. These modes appear at 3440 and 3360 cm^{-1} in aniline[9] and at 3470 and 3350 cm^{-1} in p-nitroaniline[10]. The shift towards lower frequencies in

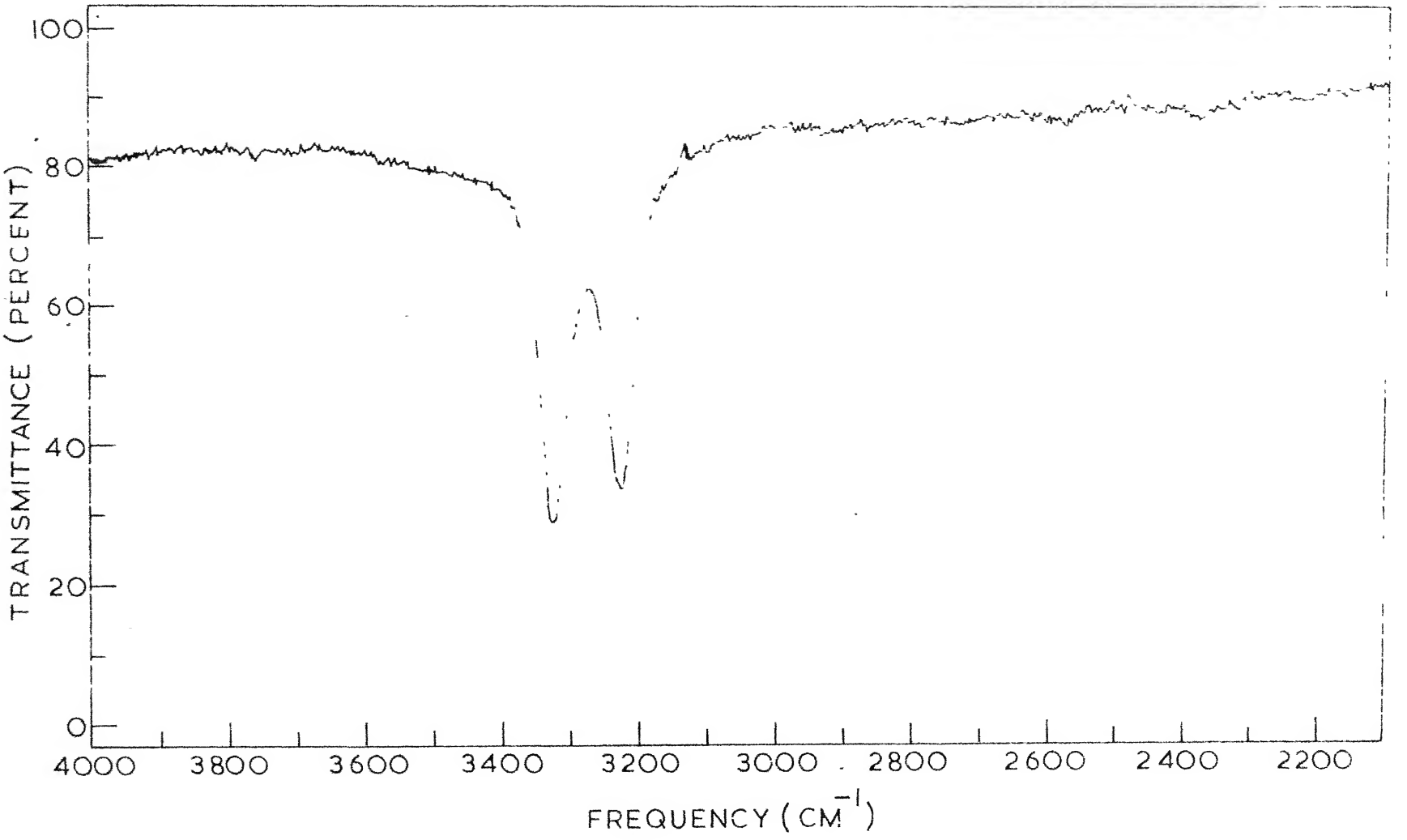

Fig. 3 Infrared spectrum of TATNB (A)

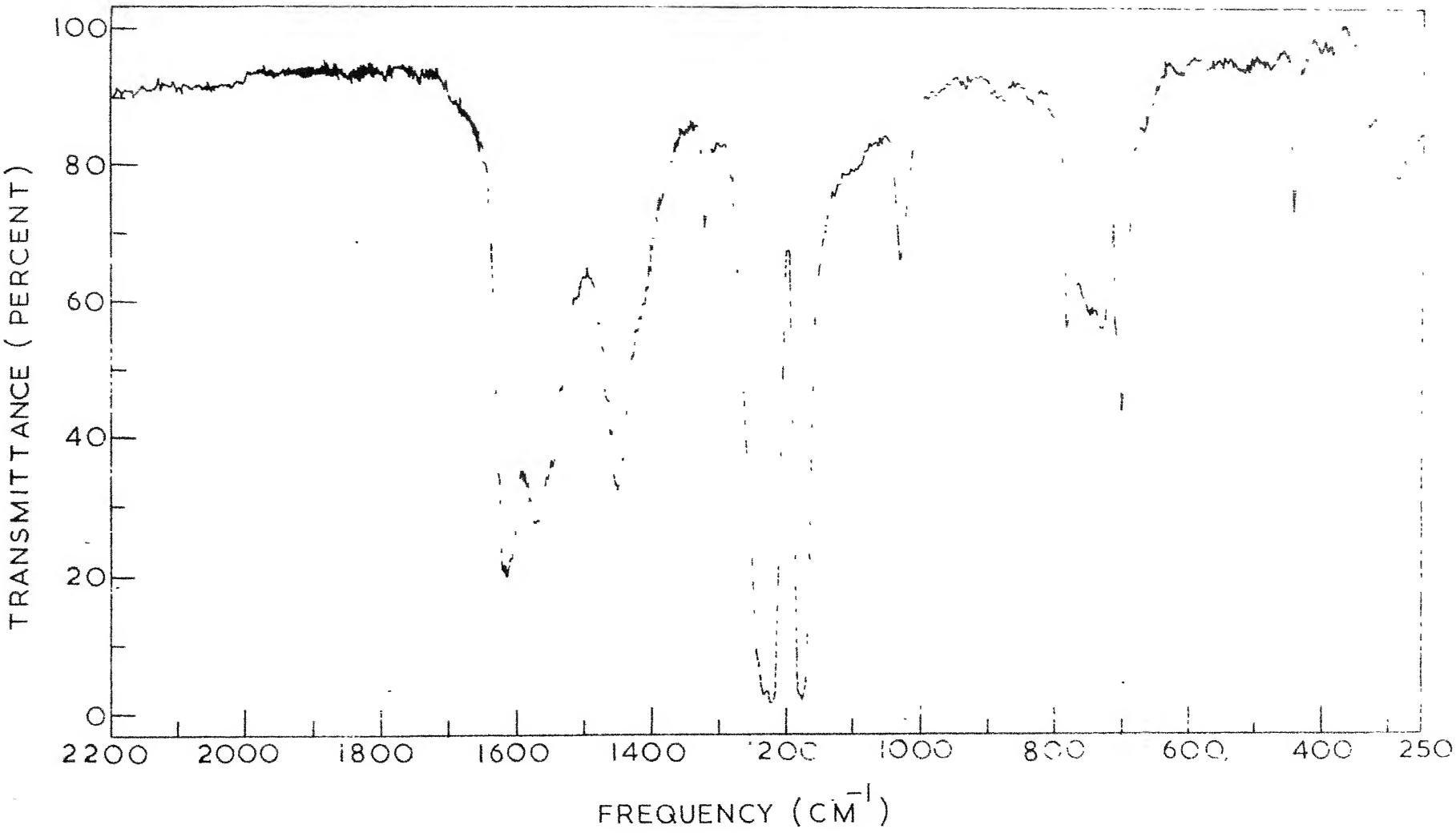

Fig. 4 Infrared spectrum of TATNB (B)

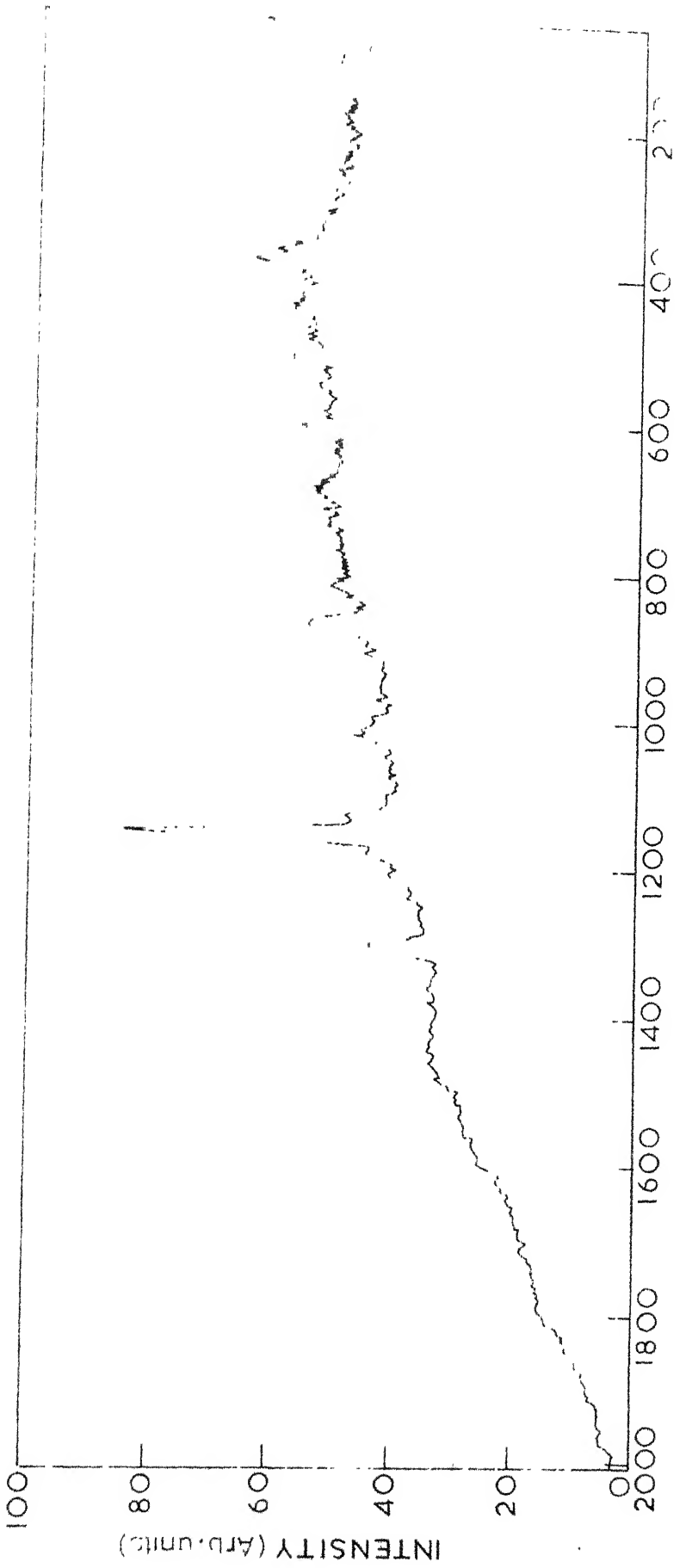

Fig. 5 Raman spectrum of TATNB

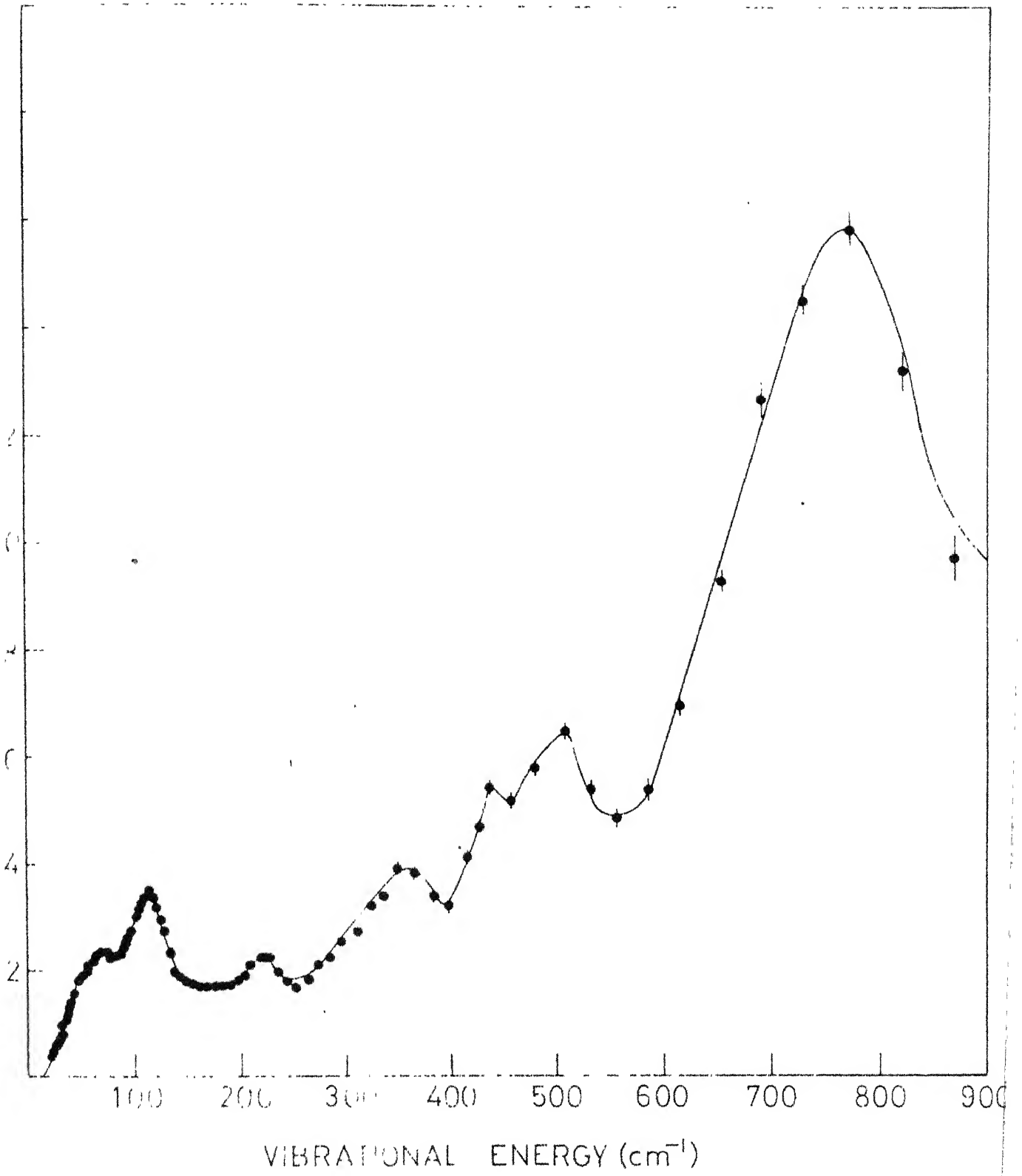

Fig. 6 Inelastic neutron spectrum of TATNB

TABLE 5

CALCULATED AND OBSERVED FREQUENCIES FOR TATNB[a]

(a) In-plane modes

Species	Calculated	Observed	Experiment	Assignment[b]
A_1'	3227	-	-	NH_2 Sy. Stretch
	1618	-	-	NH_2 Sy. Bending
	1250	1303	Raman	NO_2 Sy. Stretch
	1141	1154	Raman	X - Sens. (C–NH_2) Stretch
	1017	1017	Raman	X - Sens. (C–NO_2) Stretch
	678	687	Raman	NO_2 Sy. Bending
	476	510	Raman	X - Sens. $\phi(C–C–C)_H$
	243	236	Raman	X - Sens. $\phi(C–C–C)_O$
A_2'	3329	-	-	NH_2 Asy. Stretch
	1544	-	-	NO_2 Asy. Stretch
	1411	-	-	Ring Stretching
	1130	1129	Raman	NH_2 Rocking
	823	-	-	$\phi(C–C–N)_H + \phi(C–N–H)$
	421	430	Neutron	NO_2 Rocking
	203	-	-	X - Sens. $\phi(C–C–N)_O$

..(Contd.)

a,b (See footnote at the end of the table).

Table 5 (contd.)

(a) In-plane modes

Species	Calculated	Observed	Experiment	Assignment[b]
E'	3329	3328	I.R.	NH_2 Asy. Stretch
	3227	3227	I.R.	NH_2 Sy. Stretch
	1618	1618	I.R.	NH_2 Asy. Bending
	1572	1571	I.R.	NO_2 Asy. Stretch
	1468	1447	I.R.	Ring Stretching
	1312	1322	I.R.	Ring Stretching
	1228	1229	I.R., Raman	NO_2 Sy. Stretching
	1029	1033	I.R.	NH_2 Rocking
	907	880	Raman, I.R.	X - Sens. (C—NH_2) Stretch
	731	725	I.R.	NO_2 Bending
	589	606	Raman, I.R.	X - Sens. (C—NO_2) Stretch
	447	445	I.R., Raman	NO_2 Rocking
	354	360	Neutron, Raman	X - Sens. $\phi(C—C—N)_H$
	240	-	-	X - Sens. $\phi(C—C—C)_O$
	126	125 ?	Raman	X - Sens. $\phi(C—C—N)_O$

.. (Contd.)

Table 5 (contd.)

(b) Out-of-plane modes

Species	Calculated	Observed	Experiment	Assignment[b]
A_1''	219	220	Neutron	$(C-NH_2)$ Torsion
	148	-	-	$(C-NO_2)$ Torsion
A_2''	799	782	I.R.	NH_2 Out of plane wagging
	572	567	I.R.	NO_2 Out of plane wagging
	507	510	Neutron, I.R.	Ring distorsion
	189	-	-	(C—C) Torsion
	74	-	-	Ring distorsion
E''	805	819	Raman	NH_2 Out of plane wagging
	601	606	Raman	NO_2 Out of plane wagging
	388	381	Raman	Ring distorsion
	302	-	-	Ring distorsion
	215	212	Raman	$(C-NH_2)$ Torsion
	169	173	Raman	$t(C-C) + t(C-N)_0$
	117	125 ?	Raman	$t(C-NO_2) + t(C-C)$ or Lattice Mode

[a] All frequencies are in cm^{-1}.

[b] ø, deformation mode; t, torsional mode; Sy., Symmetric; Asy., Asymmetric; Sens., Sensitive.

TATNB is due to (a) intra and inter molecular hydrogen bonding and (b) due to resonance character of the amino group. Resonance forms of TATNB are shown in Figure 7. The empirical relations between the $\upsilon^{*}_{as}(NH_2)$ and $\upsilon_s(NH_2)$ modes for amines[11] do not hold for TATNB. The obvious reason is due to large perturbations and crowding of molecules in the crystal. However, the broadening of half-widths is in conformity with hydrogen bonding[12]. In case of bending and other modes the shift due to hydrogen bonding is in the opposite direction. The H—N—H angle bend appears at 1618 cm^{-1} and the rocking, wagging and torsional modes are at 1033, 782 and 220 cm^{-1} respectively. The last two assignments are justified from the neutron spectrum in which the intensity of a mode is weighted according to the amplitude of motion of the hydrogen atoms. One would expect larger displacements in wagging rather than torsional modes. Hence the peak at 760 cm^{-1} in the neutron spectrum is more likely due to NH_2 wagging motion and one at 220 cm^{-1} due to torsional motion. The peak at 760 cm^{-1} appears broad due to the anharmonicity arising from hydrogen bonding of the protons. This mode is also seen in I.R. spectrum at 782 cm^{-1}. In aniline[9] NH_2 wagging, rocking and torsional modes appear at 670, 1050 and 220 cm^{-1} respectively. NH_2 rocking (A_2' mode)

---

* υ_{as}: Asymmetric stretch; υ_s: Symmetric stretch.

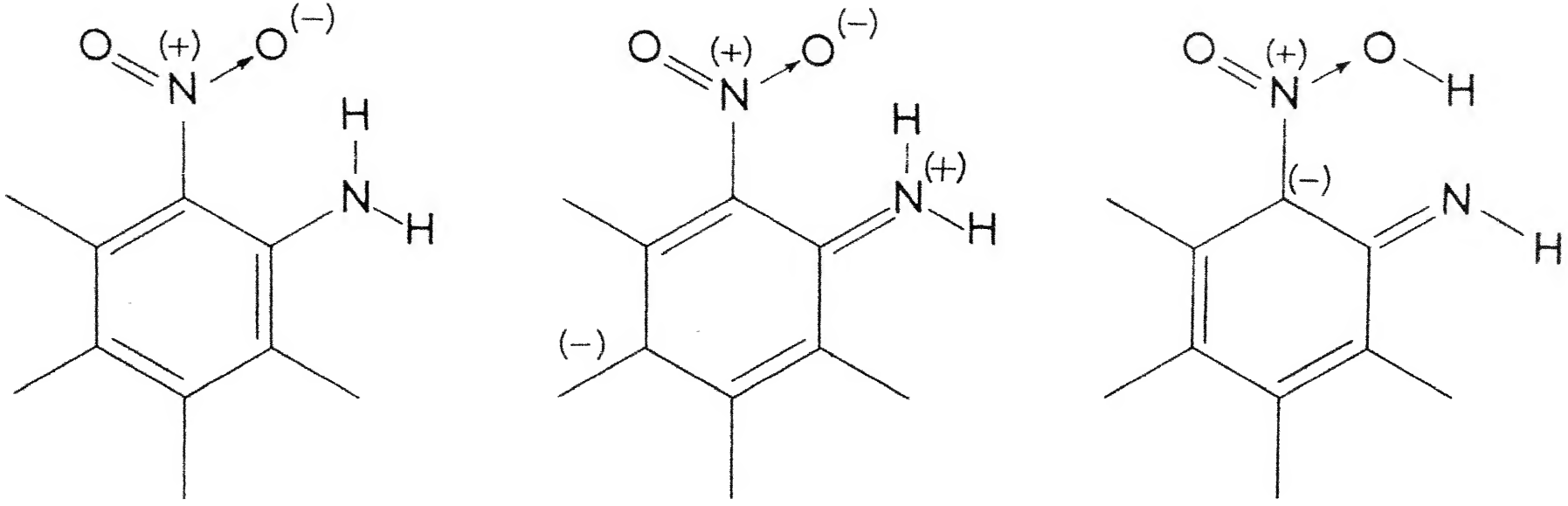

IIT R
422153

Fig. 7 Resonance forms of TATNB

appears in calculations at 1130 cm^{-1} and the weak Raman band at 1129 cm^{-1} should correspond to this mode. Though, A_2' species is Raman inactive, the appearance of this mode could be due to departure from complete symmetry of the molecule.

NO_2 Group Frequencies

NO_2 group symmetric and antisymmetric stretch frequencies have been observed in the narrow range of (1338-1355) cm^{-1} and (1510-1555) cm^{-1} respectively in para substituted nitrobenzene derivatives[13]. The Raman band at 1302 cm^{-1} should correspond to totally symmetric NO_2 stretch mode. All the totally symmetric modes are expected to appear strong in Raman spectrum. A shift towards lower frequencies is a result of strong hydrogen bonding in the molecule. Such a situation is also seen in case of hydrogen bonded O-nitrophenol where, ν_s falls to 1320 cm^{-1}. A study of a series of multiply-substituted nitro-benzene compounds shows that the bands corresponding to (NO_2) stretch appear in the I.R. spectrum with fairly large intensity. Two intense bands at 1229 and 1181 cm^{-1} may be because of degenerate ν_s (NO_2) mode. Splitting of the degenerate mode arises because the effective symmetry of a single constituent molecule in the crystal may be lowered on account of its environment and selection rules for free molecule may no longer be obeyed. Departure from the normal range of the asymmetric (NO_2) stretch mode is

either as a result of heavy multiple substitution or steric effects. In 1,3,5-trinitrobenzene this mode appears at 1557 cm^{-1} while 1,2,3-trinitrobenzene has two bands at 1558 and 1572 cm^{-1} [13]. The non-degenerate and degenerate $\nu_{as}(NO_2)$ bands in our calculations are obtained at 1544 and 1572 cm^{-1} respectively. However, only the latter mode is observed in I.R. and has a large mixing in potential energy with (C—C) stretch (as seen from the calculations). Hydrogen bonding has little effect on $\nu_{as}(NO_2)$ band and even in O-nitrophenol the ν_{as} band is at 1537 cm^{-1}.

There is a controversy about the assignment of (NO_2) symmetric bending of nitrobenzene. Green et al.[14] have assigned this mode at 677 cm^{-1} while Stephenson et al.[15] assignment corresponds to a mode at 850 cm^{-1}. In 1,3,5-trinitrobenzene[16] the mode appears in Raman spectrum at 714 cm^{-1} and favours the assignment of Green at al. The band at 687 cm^{-1} in Raman scattering of TATNB has been assigned to totally symmetric (NO_2) bending mode. The absorption bands in I.R. spectrum at 701 and 725 cm^{-1} corresponds to the degenerate (NO_2) bending mode. The shift towards somewhat higher frequencies is due to hydrogen bonding. The out-of-plane wagging mode of NO_2 group is expected to have higher frequency than in-plane mode because (a) the moment of inertia of the group about an axis perpendicular to its plane is much greater than that about an axis in its own plane

and (b) the repulsion in P.E. function for the out-of-plane mode is probably greater than that of the in-plane mode. Hence the band at 445 cm^{-1} is assigned to the in-plane rocking mode (E'), this band appears in Raman shifts at 444 cm^{-1}. A weak I.R. mode at 569 cm^{-1} is assigned to NO_2 out-of-plane wagging which is confirmed by the assignments of the nitrobenzene at 532 cm^{-1}. In 1,3,5-trinitrobenzene[17] the in-plane rocking and out-of-plane wagging modes appear at 450 and 518 cm^{-1} respectively. The corresponding degenerate mode $\omega(NO_2)$ could be Raman band at 606 cm^{-1}. NO_2 torsional mode appears at 139 cm^{-1} in nitrobenzene[15] and our calculations give at 148 cm^{-1} (A_1'' species). Some alternative assignments have been suggested for NO_2 torsional mode[18-20]. But still it seems that no definite assignment of this mode has been made.

X-Sensitive Modes

1 Stretching Modes

A study of symmetric-trihalogen substituted benzene compounds[7] shows that x-sensitive stretching modes lie in a broad range and when these compounds are deuterated completely they shift towards lower frequencies. In TATNB since all the hydrogens are replaced by NH_2 and NO_2 group symmetrically, we expect the x-sensitive frequencies to lie in the lower frequency side of the above range. However, one should be cautious in comparing these frequencies with normal (C—N) stretches, since in such cases the stretching

of (C—N) bond will necessarily involve ring stretching and motion of hydrogens or oxygens as the case may be. The sharp Raman band at 1154 cm^{-1} has been assigned to ($C—NH_2$) stretching mode (A_1'). All the totally symmetric modes are expected to appear strongly in Raman spectrum. A very large intensity in this band is because of large degree of covalent character. Since the change in polarizability during stretching is related to the extent to which electrons are shared in the bond i.e. the bond order. ($C—NO_2$) x-sensitive stretching mode will be expected to be lower than ($C—NH_2$) mode and as such has been assigned at 1019 cm^{-1}. The potential energy contributions in these modes are only 48% and 19% from ($C—NH_2$) stretch and ($C—NO_2$) stretch respectively. In the Raman spectrum of 1,3,5-trinitrobenzene[16] the ($C—NO_2$) stretch mode has not been observed because of its low intensity. The corresponding degenerate modes could be 880 and 606 cm^{-1} from Raman shifts, supported by calculations.

2 Bending and Deformation Modes

The neutron peaks at 430 and 360 cm^{-1} have been assigned to $(C—C—N)_H$ deformation modes on the basis of shift in the Raman scattering, $(C—C—N)_H$ bending frequency in aniline and normal mode calculations. The $(C—C—C)_{H,O}$ bending modes have been designated as x-sensitive since they involve considerable (C—N) stretching. They have been assigned at 510 cm^{-1} and 236 cm^{-1} from Raman scattering. The modes are in expected

region as seen from nitrobenzene[14], aniline[9] and p-nitro-aniline[10]. The sharp though weak peak in the neutron spectrum at 510 cm^{-1} could arise due to either out-of-plane wagging motion of the nitro-groups or the ring deformation arising from the out-of-plane motions of the nitrogens of the nitro and amino group[14]. The latter is more likely to involve the displacement of protons and hence expected to appear in inelastic neutron scattering.

Ring Modes

The ring stretching modes (E' species) have been assigned at 1447 and 1333 cm^{-1} from I.R. spectrum. A considerable lowering of these modes from the benzene stretching modes is as expected since there is a large increase in (C—C) bond length in TATNB (1.441 Å). A mode at 1017 cm^{-1} from Raman scattering corresponds to ring breathing mode of benzene, but as this mode involves considerable (C—N) stretch, it has been classified as x-sensitive stretching mode discussed above. The out-of-plane ring distortion mode is expected below 250 cm^{-1} which is the limit of Perkin Elmer equipment.

The peak at 110 cm^{-1} and broad band with a maximum at 65 cm^{-1} in neutron spectrum are in the region of lattice modes involving the stretching and bending of hydrogen bonds and spread nearly over the region of lattice modes observed in other hydrogen bonded systems. Raman shifts also support this.

Diagonal elements of the mean square amplitude matrix have been calculated using relation (2.23). A spatial representation of some of the normal modes are shown in Figures 8 and 9. The thermodynamic parameters i.e. entropy, heat content, heat capacity and free energy for TATNB molecule are obtained from relations (2.24) to (2.29). They are given in Table 6.

At the end, it should be added that calculations on an isolated molecule is a simplified model when one considers actual conditions prevailing in solid state. This is especially true for TATNB where hydrogen bonds play an important part. The effects that would be expected if one considers the symmetry of the space group rather than point group, are discussed in the VI Chapter. The work on isolated molecule should, however, be a good starting point.

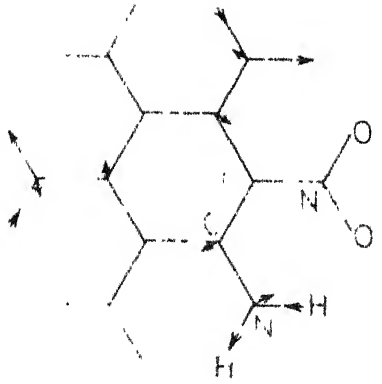

$\nu_1(NH_2)$

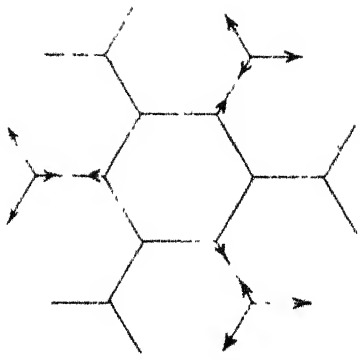

$\nu_b(NH_2)$

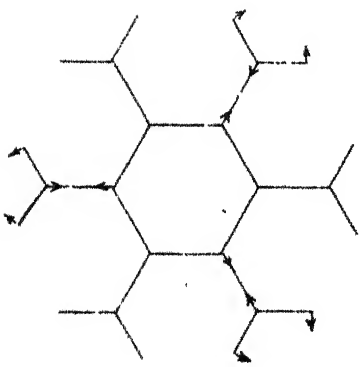

$\delta(NH_2)$

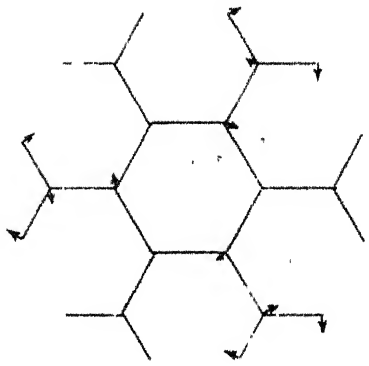

NH_2 Rocking

In plane modes

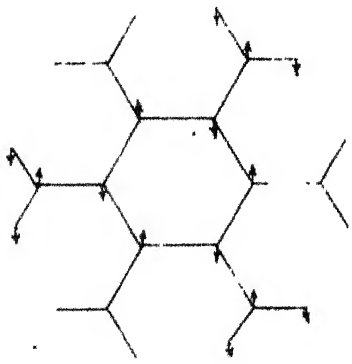

$\pi(NH_2)$

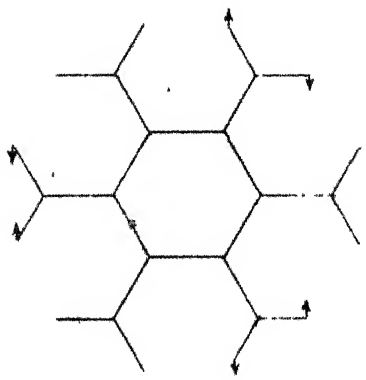

$\tau(NH_2)$

Out of plane modes

FIG. 8 A SPATIAL REPRESENTATION OF VIBRATIONAL MODES OF TATNB (A)

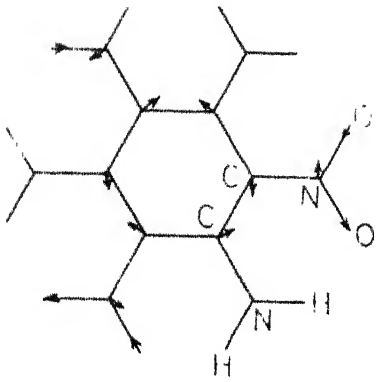

$\nu_a(NO_2)$

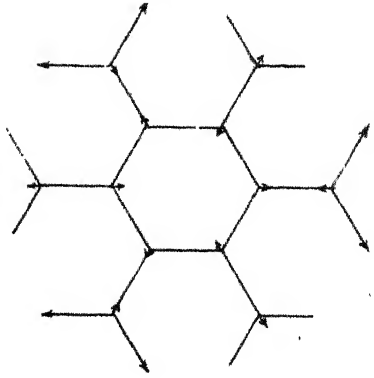

$\nu_b(NO_2)$

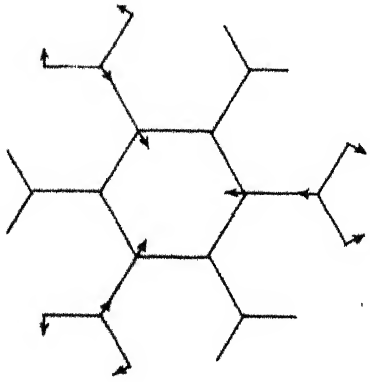

$\delta(NO_2)$

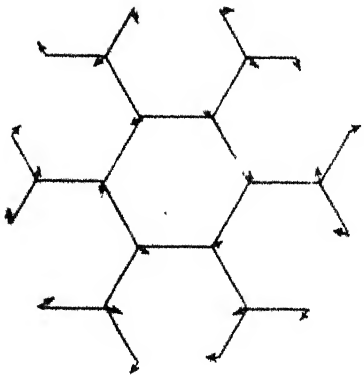

NO_2 Rock + $\delta(C-C-N)_H$

In plane modes

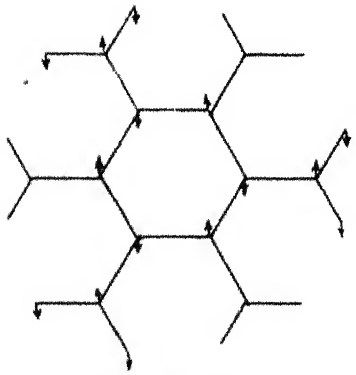

$\pi(NO_2)$

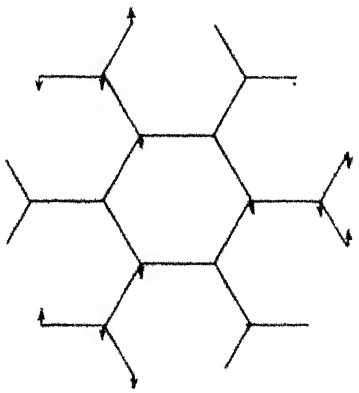

$\tau(NO_2)$

Out of plane modes

FIG. 9 A SPATIAL REPRESENTATION OF VIBRATIONAL MODES OF TATNB (B)

TABLE 6

THERMODYNAMIC QUANTITIES FOR TATNB[a]

Temp. (°A)	Heat Content $\left(\frac{H^\circ - E_o^\circ}{T}\right)$	Heat Capacity (Cp°)	Free Energy $\left(\frac{F^\circ - E_o^\circ}{T}\right)$	Entropy (S°)
300.0	39.62	68.50	88.40	128.02
400.0	48.51	81.22	101.05	149.56
500.0	56.10	91.10	112.71	168.80
573.0	60.95	96.85	120.68	181.62
600.0	62.61	98.72	123.52	186.13
700.0	68.22	104.65	133.61	201.82
800.0	73.09	109.37	143.04	216.13
900.0	77.35	113.20	151.90	229.25
1000.0	81.11	116.36	160.25	241.35

[a]All quantities are in cal./mol./° Absolute.

REFERENCES

1. H.H. Cady and A.C. Larson, Acta Cryst. 18, 485 (1965).

2. J.R. Holden, Acta Cryst. 22, 545 (1967).

3. E.B. Wilson, Jr., J. Chem. Phys. 7, 1047 (1939); 9, 76 (1941); E.B. Wilson, Jr., J.C. Decius and P.C. Cross, "Molecular Vibrations", McGraw-Hill, New York, 1955.

4. V.D. Gupta, S. Trevino and H. Boutin, J. Chem. Phys. 48, 3008 (1968).

5. J. Overend and J.R. Scherer, J. Chem. Phys. 32, 1289, 1296 (1960); 33, 446 (1960) and 34, 574 (1961).

6. J.R. Scherer and J. Overend, J. Chem. Phys. 32, 1270 (1960); 33, 1681 (1960).

7. J.R. Scherer, J.C. Evans, W.W. Mueller and J. Overend, Spectrochim. Acta 18, 57 (1960); J.R. Scherer, J.C. Evans and W.W. Mueller, Spectrochim. Acta 18, 1579 (1960).

8. D.E. Mann, T. Shimanouchi, J.H. Meal and L. Fano, J. Chem. Phys. 27, 43 (1957).

9. J.C. Evans, Spectrochim. Acta 16, 428 (1960).

10. J. Brandmüller, E.W. Schmid, H.W. Schrötter and G. Nonnenmacher, Spectrochim. Acta 17, 523 (1961).

11. P.J. Krueger, Nature 194, 1077 (1962).

12. G.C. Pimentel and A.L. McClellan, 'The Hydrogen Bond', W.H. Freeman & Co., San Francisco (1960), p. 70.

13. L.J. Bellamy, 'Advances in Infrared Group Frequencies', Methven & Co. (1968), p. 229-31.

14. J.H.S. Green, W. Kynaston and A.S. Lindsey, Spectrochim. Acta 17, 486 (1961).

15. C.V. Stephenson, W.C. Coburn and W.S. Wilcox, Spectrochim. Acta 17, 933 (1961).

16. V.G. Osipov, V.A. Shlyapochnikov and E.F. Ponizovtsev, Zh. Prikl. Spektrosk. 8, 1003 (1968).

17. H.F. Shurvell, J.A. Faniran, E.A. Symons and E. Buncel, Can. Jou. Chemistry 45, 117 (1967).

18. G. Varsanyi, S. Holly and L. Imre, Spectrochim. Acta 23A, 1205 (1967).

19. S. Nagakura, M. Kojima and Y. Moruyama, J. Mol. Spectroscopy 13, 174 (1964).

20. G.E. Campagnaro and J.L. Wood, J. Mol. Structure 6, 117 (1970).

CHAPTER - IV

SMALL-ANGLE X-RAY SCATTERING - THEORETICAL DETAILS

The folded chain lamellae with a rather uniform thickness L of between one and few hundred Å and much larger lateral extension are the main structural unit of the polymer solid. They form spherulites originating from primary crystallization nuclei which, by secondary nucleation and to a large extent by non-crystallographic branching, grow first into a bundle-like and later into a radial arrangement of ribbon-like, more or less twisted, lamellae. The size and perfection of spherulitic structure depend on crystallization conditions, on temperature, density of nuclei, impurity concentration, and so on. The parallel stacking of lamellae creates a nearly ideal periodic lattice which, due to large period L, gives rise to small-angle X-ray scattering. The intensity of scattering depends on the square of the electron density difference between the crystal lattice and the region between the adjacent crystals, which contains chain folds, tie molecules and free ends of chains incorporated only partially in the crystalline lattice. The thickness of the density-deficient layer is the second factor affecting the scattering intensity. Small-angle X-ray scattering, however, does not yield any information about the fine structure of the inter-crystal layers, particularly whether they are amorphous or not, how many and how long the folds are and so on.

For polyethylene, layer like structure was first indicated in 1956 by Claver et al.[1] who compared the free surface of a bulk sample to a fanned deck of cards. Later, the occurrence of layers was directly confirmed by electron-micrographs, both of fracture surfaces[2] and of ultramicrotome sections[3] and also by electron-microscopic examination of the debris obtained by oxidation of polyethylene with fuming nitric acid[4]. A detailed analysis of small-angle X-ray scattering curve can reveal information about the arrangement of crystalline and amorphous regions within the layers.

A reasonable-model calculations can be performed to explain the scattering curve. If the model is correct, the parameters of the model can be varied to make the calculated scattering curve fit the experimental one. However, for the studies of semicrystalline materials it appears advantageous to calculate the Fourier transform of the scattering curve as an intermediate step. The Fourier transform of the scattering curve gives the position-correlation function as introduced by Debye and Bueche[5]. The correlation function is proportional to the autoconvolution of electron density variations in the sample and can be evaluated for an assumed model. The calculated correlation function can be compared with that derived from the experimental scattering curve and the variables of the model can be best adjusted.

EXPERIMENTAL CORRELATION FUNCTION

The intensity of small-angle scattering from a single region of parallel layers along normal direction is represented by an intensity function $i(s)$ in reciprocal space. This is given by

$$i(s) = 2V \int_0^\infty \gamma'(x) \cos 2\pi xs \, dx \qquad (4.1)$$

where

$$\gamma'(x) = \int_0^\infty \eta(\xi - x)\, \eta(\xi)\, d\xi \qquad (4.2)$$

and $s = \frac{2 \sin \theta}{\lambda}$

V = Irradiated volume of the region under consideration

x = Coordinate perpendicular to the layer

θ = Half-angle of diffraction

λ = Wave-length of X-rays

$\eta(\xi)$ = Local fluctuations of electron density around the average value.

From equation (4.1), we get

$$\gamma'(x) = \frac{1}{2V} \int_0^\infty i(s) \cos 2\pi xs \, ds \qquad (4.3)$$

and $$\gamma'(0) = \langle \eta^2 \rangle = \frac{1}{2V} \int_0^\infty i(s)\, ds \qquad (4.4)$$

$\langle \eta^2 \rangle$ is the average of the square of the electron density fluctuations.

The correlation function as defined by Debye and Bueche[5] is,

$$\gamma(x) = \frac{\langle \eta_1 \cdot \eta_2 \rangle}{\langle \eta^2 \rangle} = \frac{\gamma'(x)}{\gamma(0)} \; ; (-1 < \gamma(x) < +1) \qquad (4.5)$$

When all orientations of the sets of layers are present, the measured intensity $I(s)$ has spherical symmetry and is related to $i(s)$ by

$$I(s) \sim i(s) \,/\, 4\pi s^2 \qquad (4.6)$$

The relation between $\gamma(x)$ and the experimental scattering curve obtained from relations (4.3) to (4.6) is given by

$$\gamma(x) = \frac{\int_0^\infty s^2 I(s) \cos(2\pi x s)\, ds}{\int_0^\infty s^2 I(s)\, ds} \qquad (4.7)$$

Using the experimental intensities $I(s)$, the position correlation function can be obtained from the relation (4.7). Some difficulties are involved in evaluation of this equation. Experimental scattering curve can only be obtained from a lower limit of the scattering angle. The full small-angle scattering curve is obtained by extrapolating to zero-angles the observed curve. It is found that the method of extrapolation has very little effect on the relevant part of the correlation function, neither the position nor the height of the first maximum is seriously affected, not even if absurd methods of extrapolation are used. However, the tail of the scattering curve does affect the correlation curve,

specially at small values of x. In order to correct for the overlap of the small and large angle scattering curves, the base line is assumed tangential to the tail end of the experimental curve. The part of the correlation curve affected by this procedure is shown dotted (V Chapter - Figures 17 and 18).

THE CORRELATION FUNCTION FROM A MODEL

A layer structure model with alternate high and low electron density is assumed. These layers are designated as crystalline and amorphous, though the use of these names do not imply that the crystalline layers are entirely crystalline or the amorphous layers are entirely amorphous. The thicknesses of these layers are assumed to have a Gaussian distribution. If x_c and x_a be the thicknesses of crystalline and amorphous regions then normalized distribution functions around mean values c and a are given by

$$P_c(x_c) = \frac{1}{\sqrt{2\pi}\,\Delta c}\, e^{-\frac{1}{2}\left(\frac{x_c - c}{\Delta c}\right)^2} \qquad (4.8)$$

$$P_a(x_a) = \frac{1}{\sqrt{2\pi}\,\Delta a}\, e^{-\frac{1}{2}\left(\frac{x_a - a}{\Delta a}\right)^2} \qquad (4.9)$$

Δc and Δa are the widths of these functions.

$$\text{Average crystallite length, } C = \int_0^\infty x_c\, P_c(x_c)\, dx_c \qquad .. (4.10)$$

Average amorphous length, $A = \int_0^\infty x_a P_a (x_a) dx_a$ (4.11)

Crystallinity (ϕ) is defined as

$$\phi = \frac{C}{C + A} \quad (4.12)$$

Following the method of Debye, Anderson and Brumberger[6] the position correlation function for a two-phase model is given by the expression

$$\gamma(x) = \frac{p_{cc}(x) - \phi}{1 - \phi} \quad (4.13)$$

$p_{cc}(x)$ denotes the probability that if one end of a hypothetical measuring rod of thickness x is in the crystalline region (higher electron density phase) then the other end is also in one of the crystalline regions. The situation is very much simplified by the fact that the polyethylene chains are found to be normal to the layers[7-9]. Let $p_{cc}(x)$ be expressed as

$$p_{cc}(x) = q_c(x) + q_{cac}(x) + q_{cacac}(x) + \cdots \quad (4.14)$$

where $q_c(x)$ denotes the probability of finding the two ends of the measuring rod in the same crystalline region, $q_{cac}(x)$ to that of the ends being in neighbouring crystalline regions and so on.

The probability $q_c(x)$ for a length x in a crystalline region of thickness x_c is $(x_c - x)/x_c$ as

seen from Figure 10(a). For all the thicknesses x_c we get

$$q_c(x) = \frac{\int_o^\infty (x_c - x)\, P_c(x_c)\, dx_c}{\int_o^\infty x_c\, P_c(x_c)\, dx_c} \qquad (4.15)$$

For contributions to $q_{cac}(x)$ the measuring rod must be situated as shown in Figure 10(b). In this case, it is composed of three vectors x_1, x_a, x_2. According to a well known theorem[7], the distribution of such Vasum of vectors (Vector-Sum) is given by the normalized distribution function

$$P_{cac}(x) = Q(x_1) \frown P_a(x_a) \frown Q(x_2) \qquad (4.16)$$

Sign $\frown$ denotes the convolution product of the two functions. $P_a(x_a)$ is given by the equation (4.9) and $Q(x_1) = Q(x_2)$. The contributions for $Q(x_1)$ are obtained from the crystalline regions which has thicknesses more than x_1 i.e. the fraction:

$$\int_{x_1}^\infty P_c(x_c)\, dx_c$$

Normalizing this function, we get

$$Q(x_1) = \frac{\int_{x_1}^\infty P_c(x_c)\, dx_c}{\int_o^\infty \int_{x_1}^\infty P_c(x_c)\, dx_c\, dx_1} \qquad (4.17)$$

Using relations (4.16), (4.17), (4.8) to (4.11), the expression for $P_{cac}(x)$ can be written as

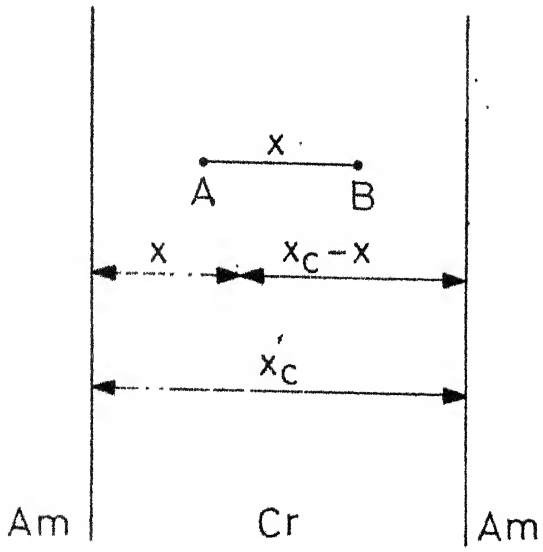

(a)

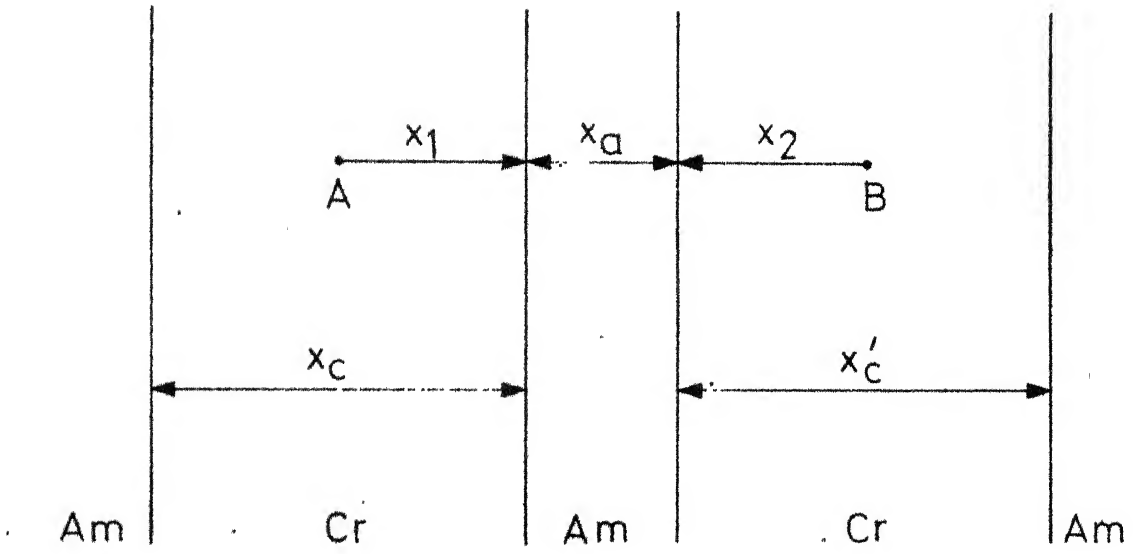

(b)

FIG. 10 POSITION OF THE MEASURING ROD A B, WHICH CONTRIBUTES TO (a) q_C (b) q_{CAC}

$$P_{cac}(x) = N' \int_{c}^{x} \left[\int_{c}^{x} \left\{ \int_{y}^{\infty} e^{-\frac{1}{2}\left(\frac{x_1 - c}{\Delta c}\right)^2} dx_1 \right\} e^{-\frac{1}{2}\left(\frac{Z-Y-a}{\Delta a}\right)^2} dy \right] \left[\int_{x-Z}^{\infty} e^{-\frac{1}{2}\left(\frac{x_2 - c}{\Delta c}\right)^2} dx_2 \right] dZ \qquad (4.18)$$

where $N' = \frac{1}{c^2} \frac{1}{(2\pi)^{3/2}} \frac{1}{\Delta a \cdot (\Delta c)^2}$

Now, the relation between $q_{cac}(x)$ and $P_{cac}(x)$ will be developed. The chain length can take only N discrete values. $q_{cac}(x)$ can be written as

$$q_{cac}(x) = \frac{T_{cac}(x)}{R_c(x)} \qquad (4.19)$$

$T_{cac}(x)$ is the number of positions of a measuring rod of length x with A and B in neighbouring crystalline layers and $R_c(x)$ is the number of positions of a measuring rod when A is in crystalline layer and B in either of layers. $R_c(x)$ is equal to ϕN per unit length. S_{cac} is the total number of vectors of type cac. This number is equal to $\phi^2 N^2 (C+A)$ per unit length. $T_{cac}(x)$ is given by :

$$T_{cac}(x) = \frac{P_{cac}(x)\ S_{cac}}{N} \qquad (4.20)$$

Putting the respective values we get

$$q_{cac}(x) = \phi(C+A)\ P_{cac} \qquad (4.21)$$

Similarly $$q_{cacac}(x) = \phi(C+A)\, P_{cacac} \qquad (4.22)$$

where $$P_{cacac}(x) = \overbrace{Q_c\, P_a\, P_c\, P_a\, Q_c} \qquad (4.23)$$

A relation similar to equation (4.18) can be written for $P_{cacac}(x)$ and higher order terms.

The expression for correlation function is obtained using relations (4.13) to (4.15), (4.21) and (4.22) and is given below:

$$y(x) = \frac{1}{1-\phi}\left[\frac{1}{C}\int_x^{\infty}(x_c - x)\, P_c(x_c)\, dx_c + \phi(C+A)\, P_{cac} + \phi(C+A)\, P_{cacac} + \cdots\cdots - \overline{\phi}\right] \qquad (4.24)$$

The theoretical correlation curve equation (4.24) has been numerically solved. Theoretical curve has been shown in Table 7 (Chapter V) for some particular values of model parameters (c, a, Δc, Δa). These parameters can be varied to get an agreement between theoretical and experimental correlation curves.

REFERENCES

1. G.C. Claver, Jr., R. Buchdahl and R.L. Miller, J. Polymer Sci. 20, 202 (1956).

2. F.R. Anderson, J. Polymer Sci. C3, 123 (1963).

3. E.H. Andrews, J. Polymer Sci. B3, 353 (1965).

4. A. Keller and S. Sawada, Makromol. Chem. 74, 190 (1964); R.P. Palmer and A.J. Cobbold, Makromol. Chem. 74, 174 (1964).

5. P. Debye and A.M. Bueche, J. Appl. Phys. 20, 518 (1949).

6. P. Debye, H.R. Anderson, Jr., and H. Brumberger, J. Appl. Phys. 28, 679 (1957).

7. P.H. Till, J. Polymer Sci. 24, 301 (1957).

8. A. Keller, Phil. Mag. 2, 1171 (1957).

9. E.W. Fischer, Z. Naturforsch 12A, 753 (1957).

10. R. Hosemann and S.N. Bagchi, "Direct Analysis of Diffraction by Matter", North-Holland Publishing Co., Amsterdam (1962).

CHAPTER - V

SMALL-ANGLE X-RAY SCATTERING FROM POLYETHYLENE AND WOOL

Morphological structure of polyethylene is a subject of considerable interest because of its importance in understanding the process of crystallization and thermodynamic behaviour. It is now almost established that polyethylene has layer like structure[1-8], but still there is much controversy about the detailed arrangement of the crystalline and amorphous regions in these layers. As seen in the last chapter, small-angle X-ray scattering depends on the difference of the square of the average electron densities between different regions. The analysis of such a scattering will give information regarding the detailed arrangement of the layers. Abundant experimental observations have been reported earlier for melt-crystallized and fibrous polyethylene samples[9-24]. Howover, the experimental observations on bulk-crystallized samples are much less. Secondly, in most of the studies the interpretation of the scattering maxima has been done assuming the Bragg condition to be valid. This is obviously not the right approach, since normally the arrangement of ordered and disordered regions is not regular. By way of example, the results obtained by Geil[23] from small-angle X-ray scattering are not in agreement with their electron-microscopic measurements. Recently, Vonk[24] et al. have reported a study of correlation functions based on a

two-phase parallel-layer model with different average electron densities. However, their results vary within wide limits. Russian workers[25] have reported results in agreement with those obtained from electron-microscope. In view of these discrepancies, it was decided to study the position correlations in a linear polyethylene sample which has been annealed just below the melting point and cooled very slowly to room temperature. To test the validity of the two-phase model the experiments are also performed on irradiated polyethylene sample.

EXPERIMENTAL

The Luzzati-Baro small-angle scattering camera[26] has been used with linear collimation system. The three slit system is used to remove parasitic scattering. The slit system is shown in Figure 11. The camera is evacuated to avoid air scattering. The alignment corresponds to a Bragg value of about 300 Å for CuK_{α} radiation. Photographic technique is used for recording the scattering pattern. Sample to film distance was 10.8 cms. for polyethylene and 11.4 cms. for wool samples. CuK_{α} radiation with nickel filters was used. Intensity measurements were made on a Kipp-Zonan microphotometer. The intensities were converted to relative scale with the help of a log-scale obtained by means of a smooth wedge. Polyethylene samples were about 1 mm thick. The X-ray patterns of Polyethylene and Irradiated Polyethylene

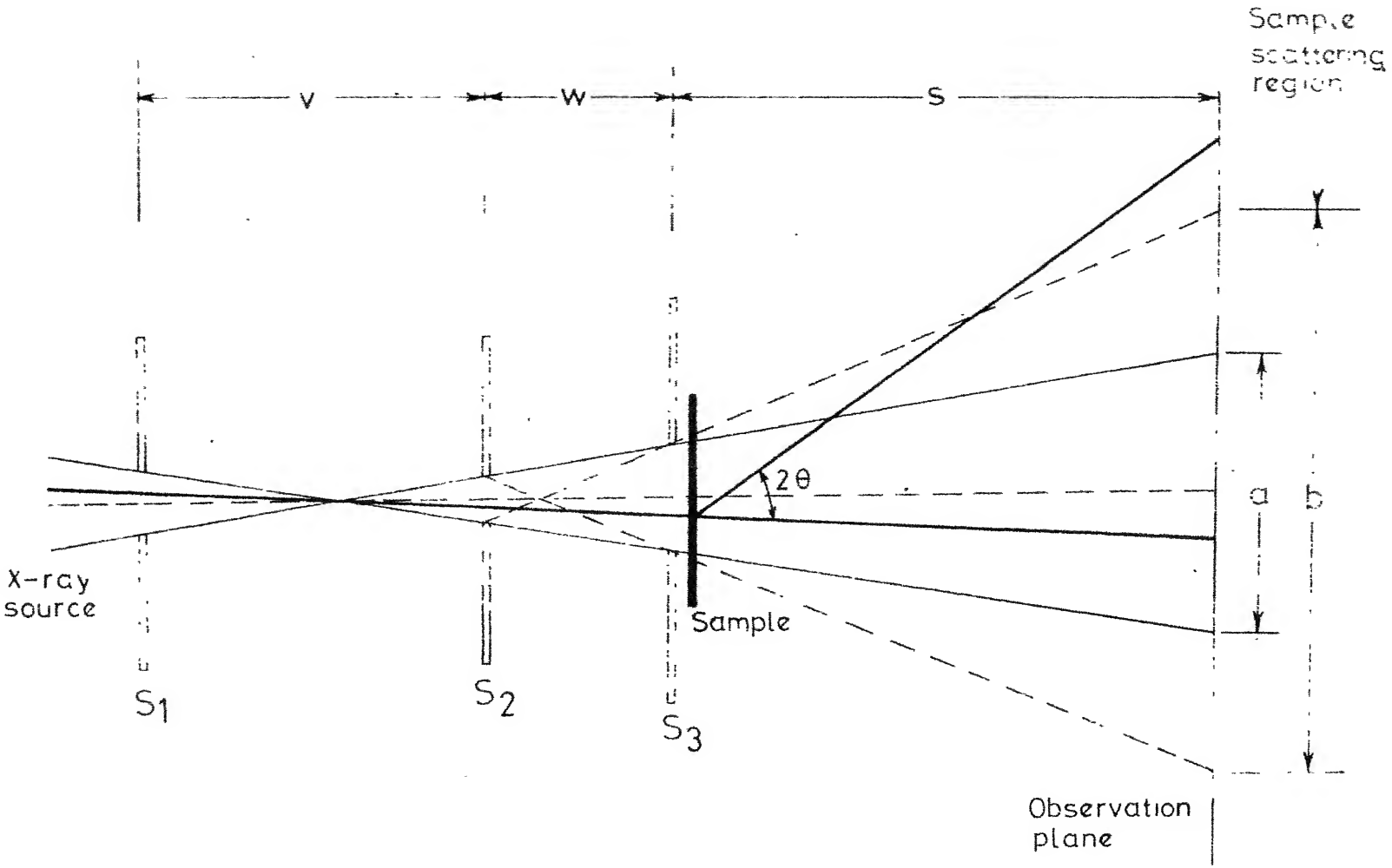

FIG. 11 SLIT SYSTEM FOR SMALL-ANGLE X-RAY SCATTERING APPARATUS.

samples and a log-scale variation are shown in Plate 1 (a,b,d) and their microphotometer records are shown in Figures 12, 13 and 14 respectively.

SLIT CORRECTION

Small-angle X-ray scattering collimation systems ordinarily use slits instead of pinholes in order to give sufficient scattered intensity. With slit collimation, at a particular angle setting of the collimation system, the detector records the scattering from a range of angles, rather than from a given angle. This imperfect collimation leads to a distortion in the scattering curve. These errors are essentially due to the width and height of the direct beam. The process of correcting the experimental scattering curve has been considered by several authors[27-37]. Some of the methods suggested need numerical differentiation of the experimental curve. Numerical differentiation can be quite inexact, specially when applied to an experimental curve which is known only approximately. Numerical calculations in these methods are tedious and time consuming. A relatively simple method has been suggested by Schmidt and Height[38] which has the advantage of eliminating the need for numerical differentiation or functional fitting of the experimental curve. For the case of infinite height and negligibly wide primary beam this method is readily applicable[39] and is used for the present slit-correction of the scattering curve.

(a)

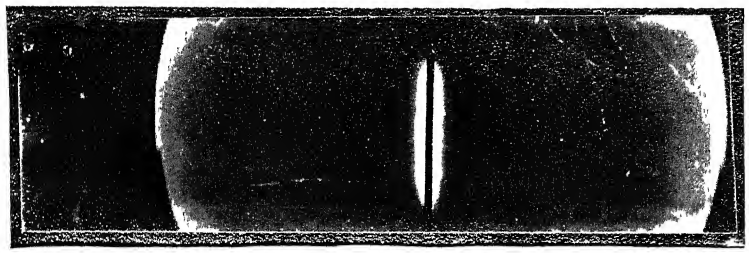

(b)

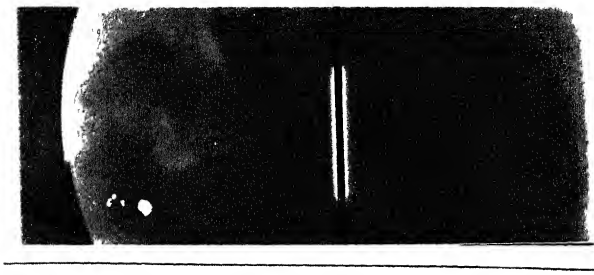

(c)

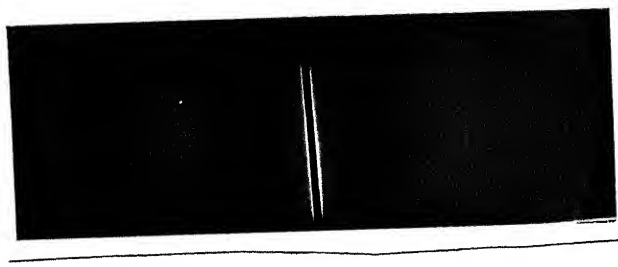

(d)

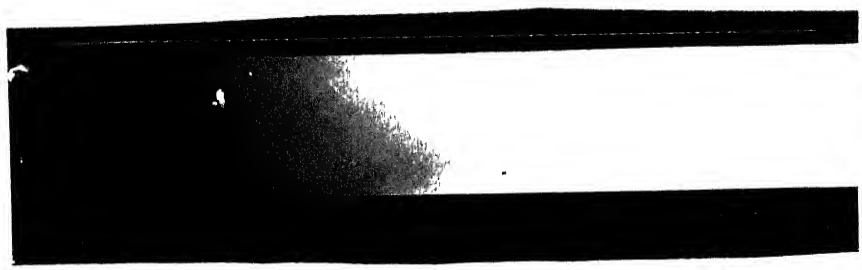

PLATE 1. Small-angle X-ray scattering from (a) Polyethylene (b) Irradiated-Polyethylene (c) Wool.

(d) Standard continuous scale for relative intensity measurements.

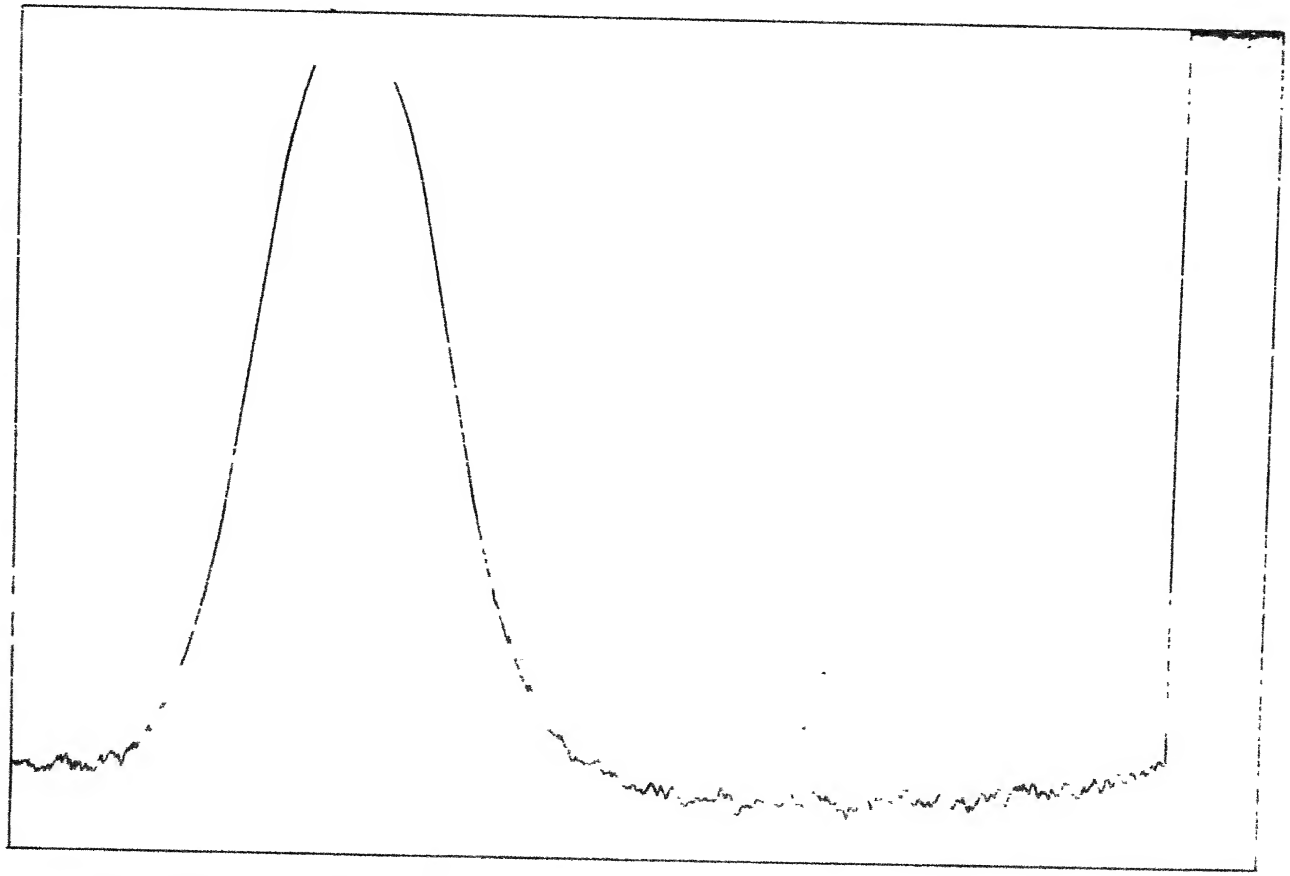

FIG. 12 MICROPHOTOMETER RECORD OF LOW-ANGLE X-RAY SCATTERING FROM POLYETHYLENE.

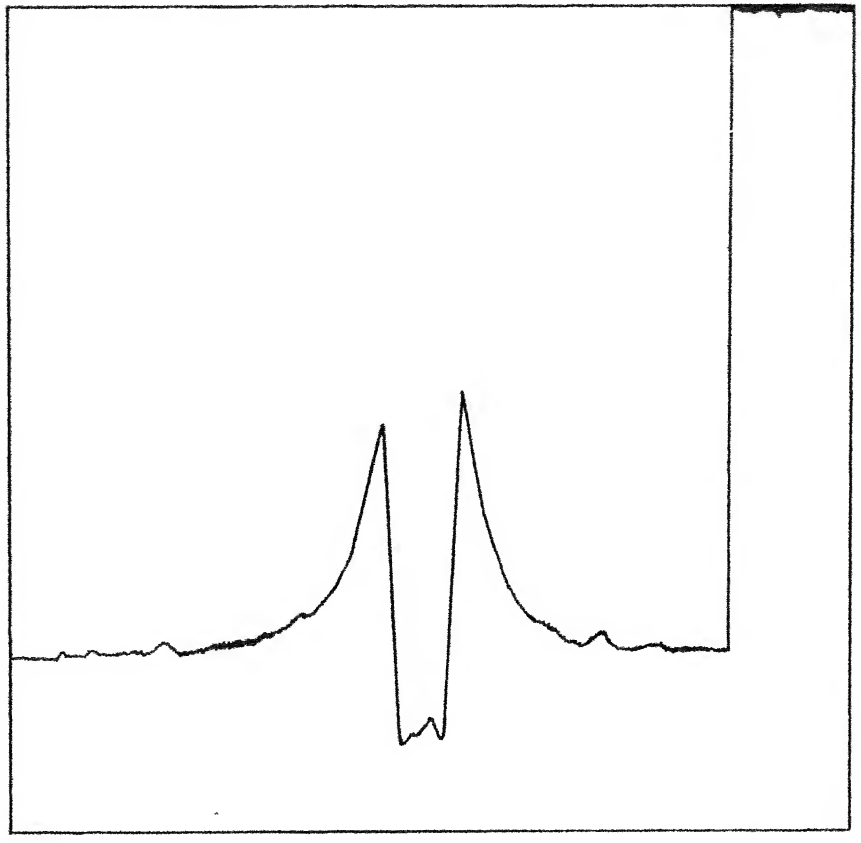

FIG. 13 MICROPHOTOMETER RECORD OF LOW-ANGLE X-RAY SCATTERING FROM IRRADIATED POLYETHYLENE

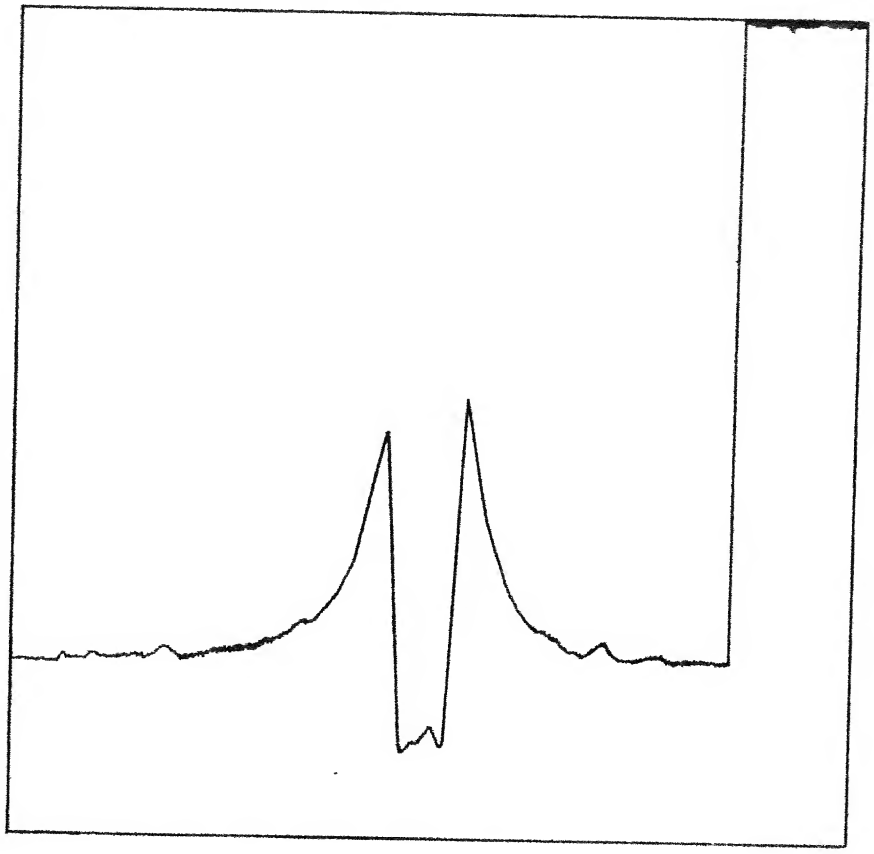

FIG. 13 MICROPHOTOMETER RECORD OF LOW-ANGLE X-RAY SCATTERING FROM IRRADIATED POLYETHYLENE

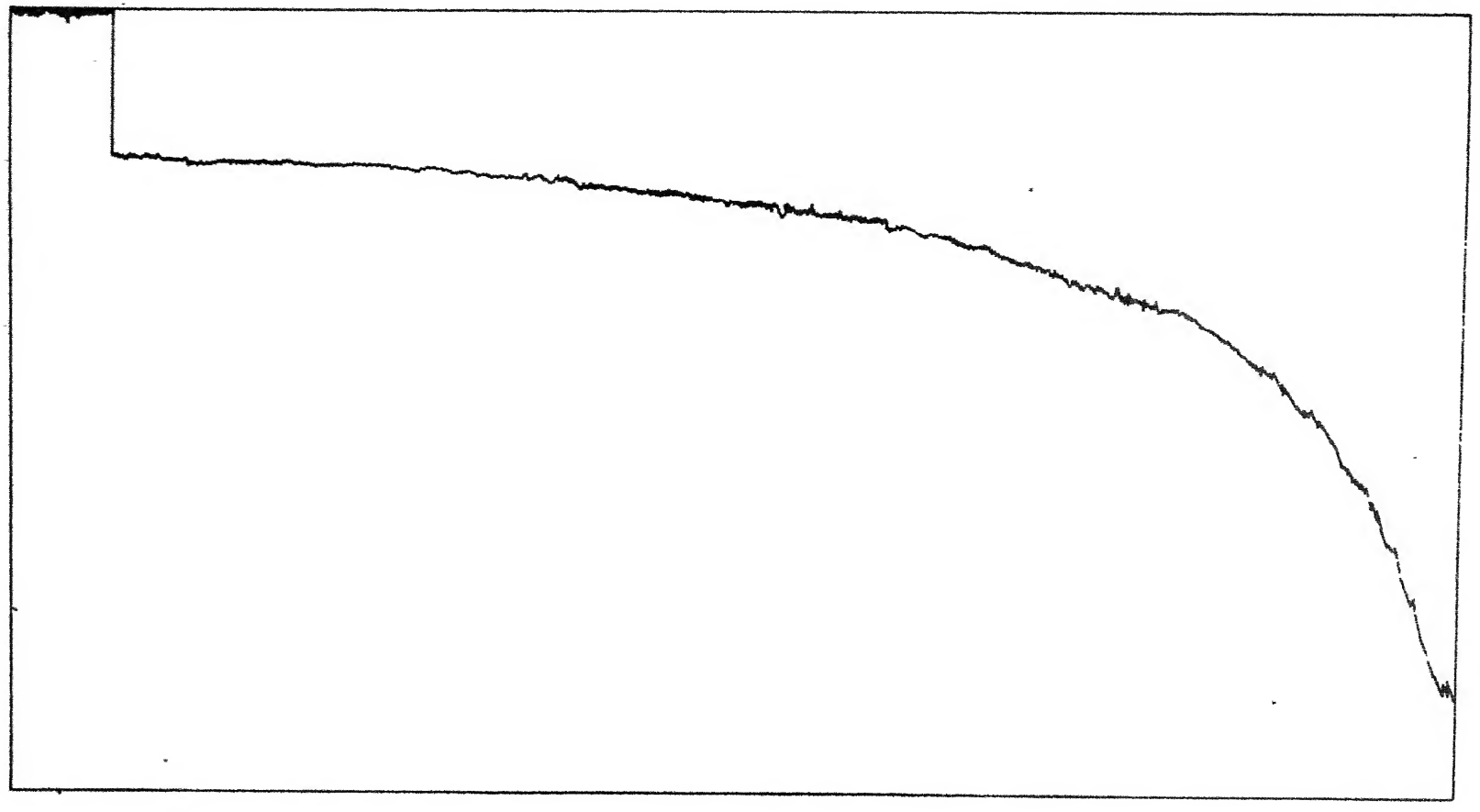

FIG. 14 STANDARD CONTINEOUS SCALE FOR RELATIVE INTENSITY MEASUREMENTS. (MICROPHOTOMETER TRACE)

Steps followed in the process are given below.

For the slits of negligible width and infinite height, the experimental scattered intensity $F(h)$ for a given angle h is related to the perfect collimation scattered intensity $I(h)$ by the relation

$$F(h) = \int_0^\infty I(h^2 + \phi^2)^{\frac{1}{2}} \, d\phi \qquad (5.1)$$

or the scattered intensity $I(h)$ can be written as[27,28]

$$I(h) = -\frac{2}{\pi} \int_0^\infty \frac{dt}{(h^2 + t^2)^{\frac{1}{2}}} F'\left[(h^2+t^2)^{\frac{1}{2}}\right] \qquad (5.2)$$

where ϕ and t in equation (5.1) and (5.2) are the variables of integration in terms of scattering angle.

Following the method of Schmidt and Height[38] above equation can be expressed as

$$I(h) \propto \frac{1}{j^2}\left[j(2j+1)^{\frac{1}{2}} F(j\Delta h) - \sum_{i=1}^{\infty} T_{ij} F\left((i+j)\Delta h\right)\right] \qquad .. (5.3)$$

where
$$h = j\Delta h$$
$$h_i = (i+j)\Delta h$$
$$T_{ij} = (\Delta h)^{-1} (i+j) \Delta_{ij}^2$$
$$\Delta_{ij} = -R_{i+1} + 2R_i - R_{i-1}$$
$$R_i = \Delta h (i^2 + 2ij)^{\frac{1}{2}}$$

Δh is taken as 5×10^{-4} radians. Summation for i is taken from 1 to 15 which gives fairly good results on a test problem. The experimental and slit corrected curves

for polyethylene and irradiated-polyethylene samples are shown in Figures 15 and 16 respectively.

RESULTS

Studies of Polyethylene Sample

The slit corrected experimental curve (Figure 15) is used for getting the position-correlation function for polyethylene sample. The relation (4.7) has been used. This curve has been plotted and shown in Figure 17. The effect of extrapolation of the experimental curve to zero-angle on the correlation function has been discussed in the previous chapter (p. 66). The essential idea is that the relevant part of the correlation curve is almost insensitive to the extrapolation. Several maxima are obtained. The position of the first maximum at 118 Å denotes an approximate repeat distance. This distance includes the widths of the crystalline and amorphous regions. Buchanann and Miller[25] have reported in polyethylene single-lamellar shadow-heights varying between 97 and 127 Å. The mean shadow-height obtained by them from measurements on fracture faces several lamellae thick is also found to be nearly 117 Å which is in general agreement with the result obtained from the correlation curve (repeat distance, 118 Å).

Correlation-curve can also be used to obtain a very rough estimate of the degree of order (ϕ) within the system.

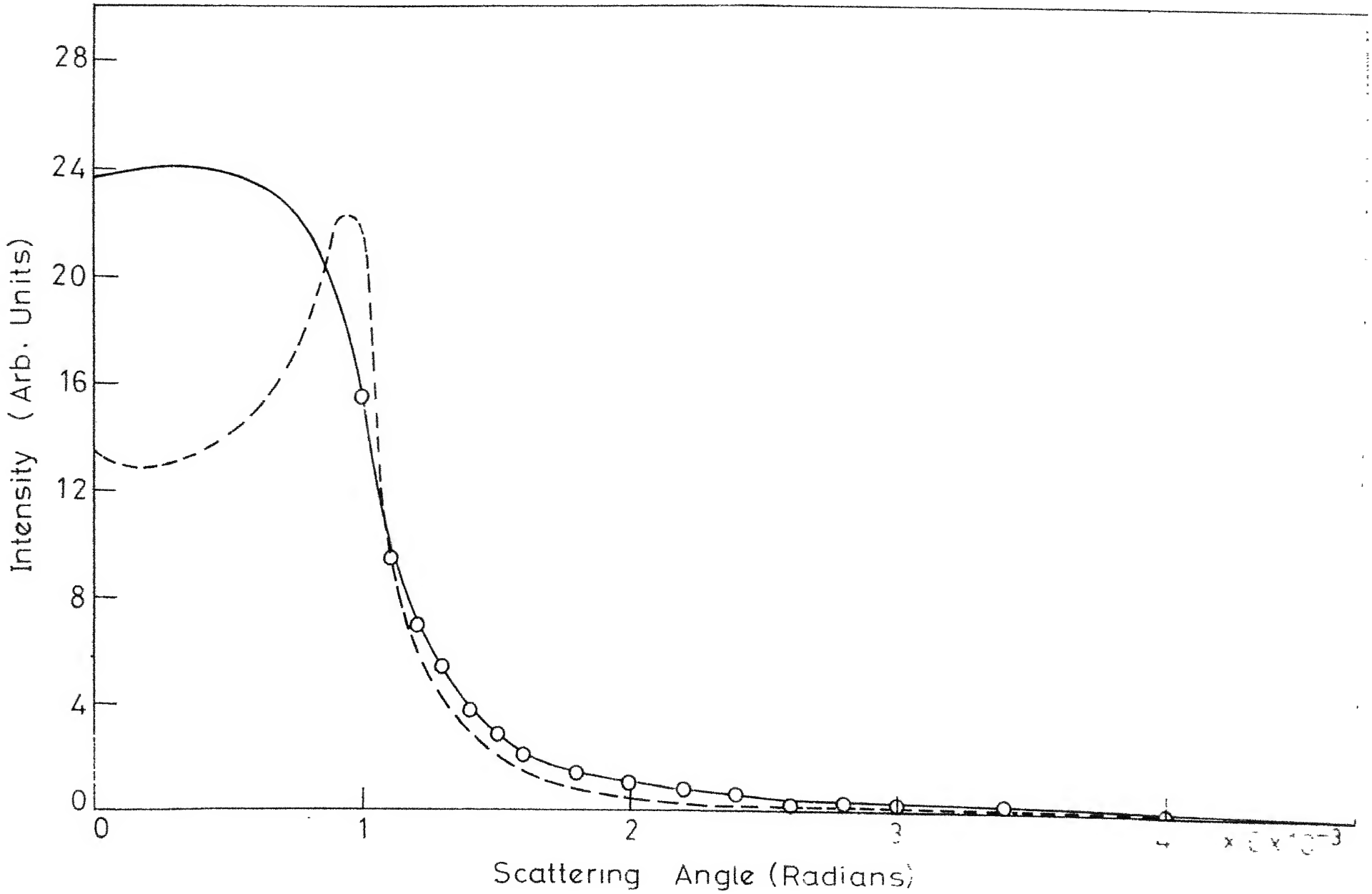

FIG. 15 OBSERVED (——) AND SLIT CORRECTED (- - -) SCATTERING CURVES FOR POLYETHYLENE.

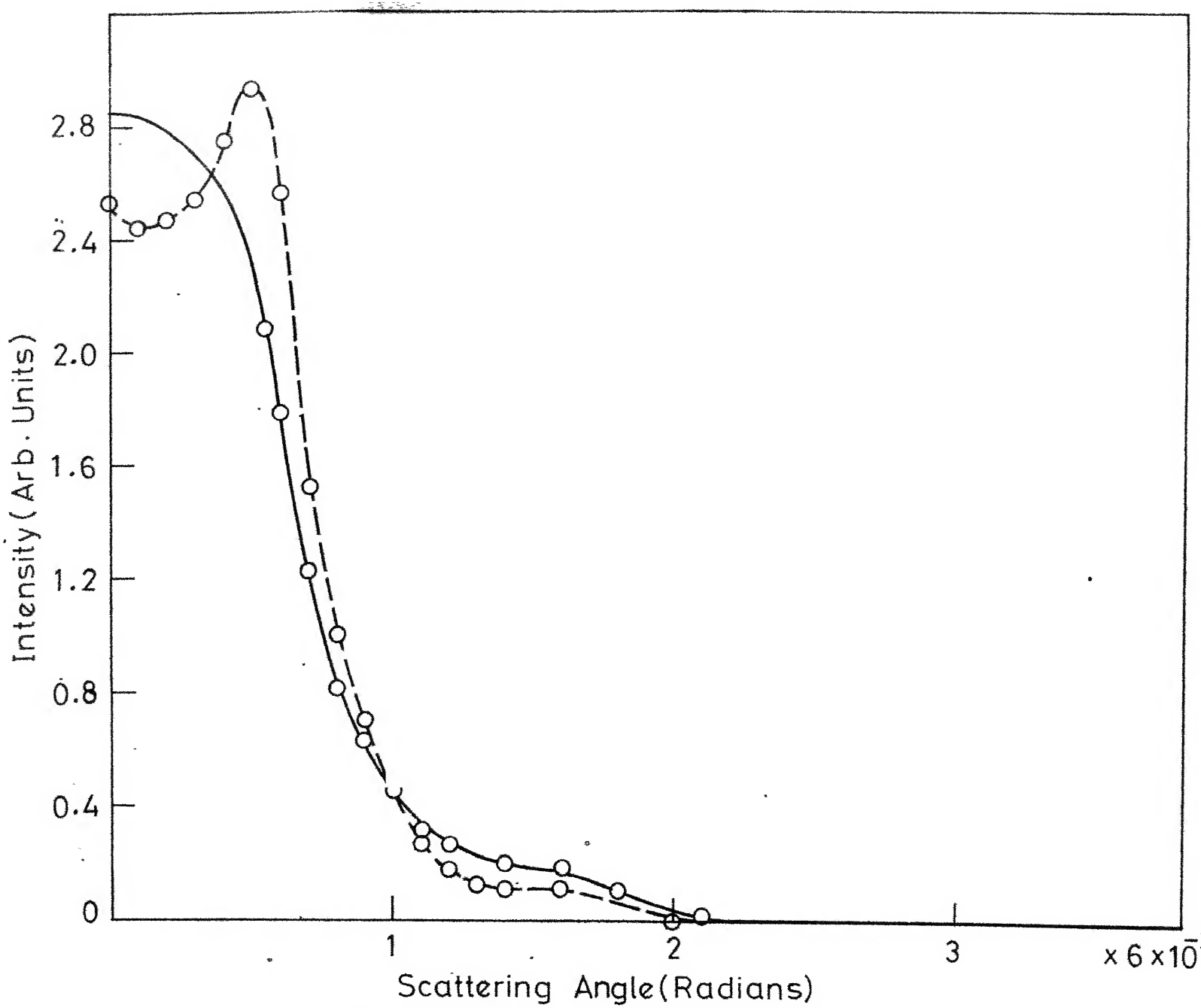

FIG. 16 OBSERVED (——) AND SLIT CORRECTED (---) SCATTERING CURVES FOR IRRADIATED POLYETHYLENE

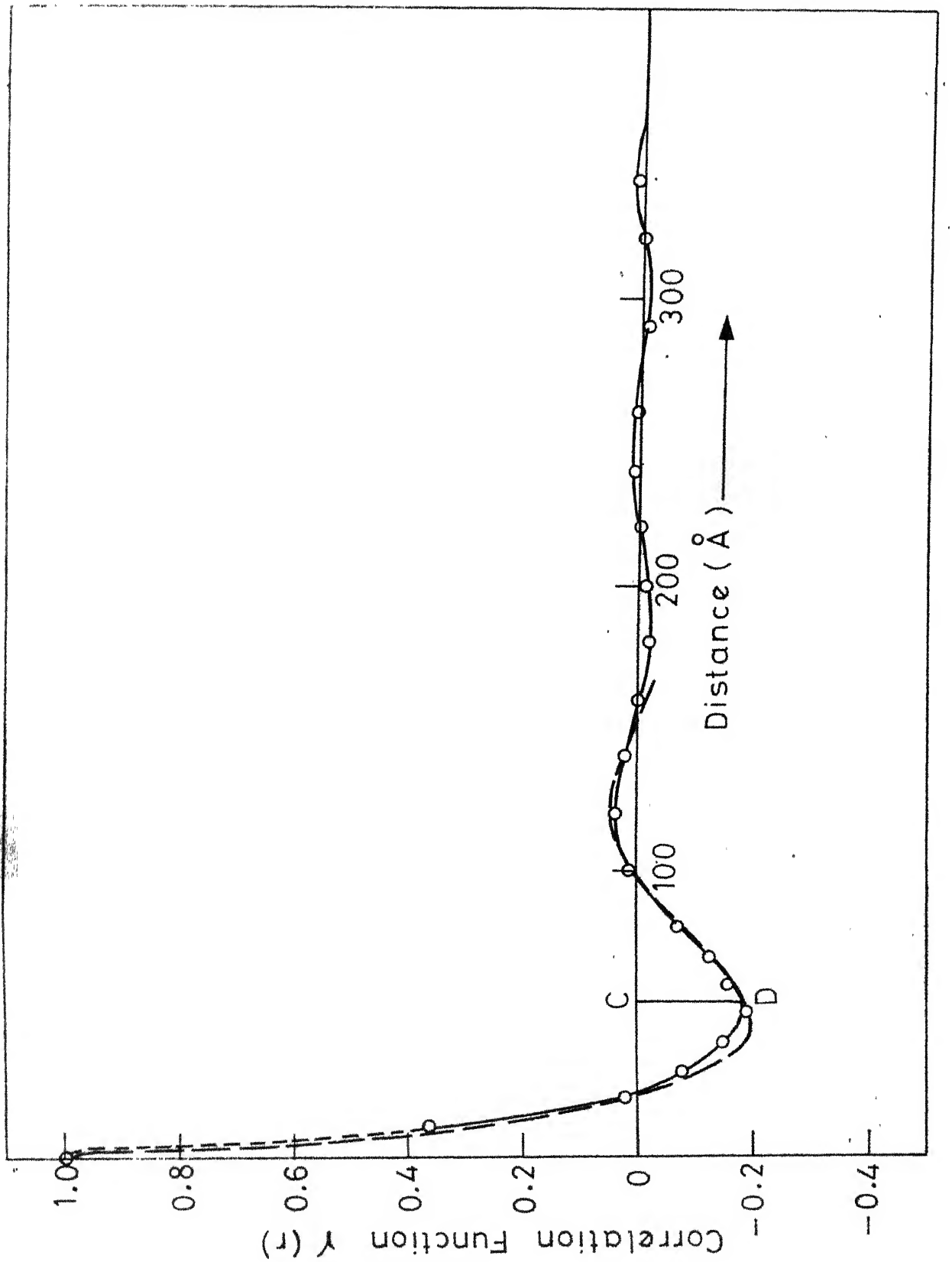

FIG. 17 EXPERIMENTAL (——) AND THEORETICAL (– –) CORRELATION FUNCTION FOR POLYETHYLENE SAMPLE

This is given by $\phi = (1+CD)^{1}$ where CD is the depth of the first minimum as shown in Figure 17. It gives a value of $\sim$ 85%. This method of estimation is based on the assumption that the distribution of thicknesses in the crystalline and amorphous regions is narrow and is peaked around the average values. The correlation function is theoretically obtained from expression (4.24). The terms upto $q_{cacac}(x)$ are used. The model parameters are the crystallinity (ϕ), the widths of the distribution functions of crystalline and amorphous regions (Δc and Δa). The long period (c+a) is taken as the position of the first maximum. The parameters of the model are varied to match the theoretical curve to the experimental correlation function. These curves are shown in Figure 17. This gives a crystallinity of 83%. The average widths of the crystalline and amorphous regions are 98 and 20 Å. The values of the theoretical correlation curve with respective terms (equation (4.24)), as a function of distance, are given in Table 7A. Buchanann and Miller[25] have reported these distances as 110 and 14 Å for 89% degree of crystallinity.

To test the validity of the two-phase model, the irradiated sample of polyethylene has been studied. The experimental and slit corrected curve is shown in Figure 16. The position-correlation curve obtained from the slit corrected scattering curve is shown in Figure 18. In the

TABLE 7

CALCULATED POSITION-CORRELATION FUNCTIONS*

(A) Polyethylene

$c = 98.0$ Å $\quad \Delta c = 35.0$ Å

$a = 20.0$ Å $\quad \Delta a = 7.5$ Å

$\phi = 83\%$

x(Å)	$q_c(x)$	$q_{cac}(x)$	$q_{cacac}(x)$	$\gamma_{the}(x)$	$\gamma_{exp}(x)$	x(Å)
0	1.000	0.000	0.000	1.000	1.000	0
20	0.797	0.030	0.000	-0.021	0.031	20
40	0.599	0.198	0.000	-0.194	-0.127	40
60	0.413	0.390	0.002	-0.154	-0.155	60
80	0.253	0.556	0.009	-0.078	-0.087	80
100	0.132	0.672	0.027	0.008	0.012	100
120	0.057	0.712	0.070	0.053	0.037	120
140	0.020	0.668	0.147	0.028	0.024	140

(B) Irradiated-Polyethylene

$c = 67.0$ Å $\quad \Delta c = 40.0$ Å

$a = 29.0$ Å $\quad \Delta a = 16.0$ Å

$\phi = 69.9\%$

x(Å)	$q_c(x)$	$q_{cac}(x)$	$q_{cacac}(x)$	$\gamma_{the}(x)$	$\gamma_{exp}(x)$	x(Å)
0	1.000	0.000	0.000	1.000	1.000	0
20	0.728	0.031	0.000	0.200	0.230	20
40	0.486	0.155	0.003	-0.182	-0.285	40
60	0.291	0.339	0.014	-0.184	-0.215	60
80	0.152	0.484	0.038	-0.084	-0.050	80
100	0.068	0.546	0.081	-0.014	-0.060	100
120	0.025	0.524	0.146	-0.012	-0.005	120

*$\gamma_{the}(x)$ = Theoretical correlation function; $\gamma_{exp}(x)$ = Experimental correlation function.

All other notations are same as given in text, Chapter IV, pages 66-72.

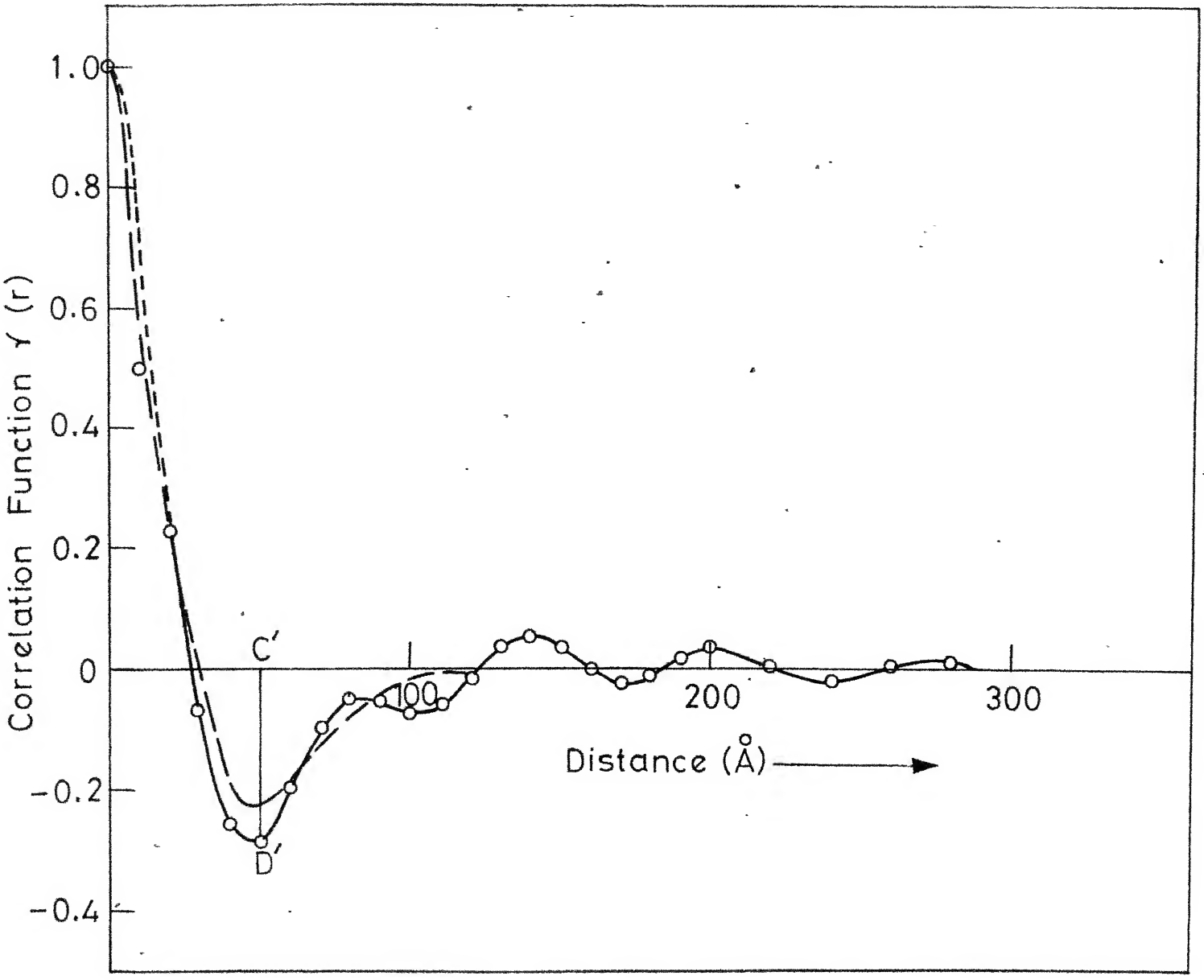

FIG. 18 EXPERIMENTAL (——) AND THEORETICAL (— —) CORRELATION FUNCTION FOR IRRADIATED POLYETHYLENE SAMPLE.

present case, the position of the first maximum is not very clear; however, it occurs at $\sim$ 84 Å. An estimate of the long range order is made from the position of the first minimum, which gives a distance of 96 Å. Crystallinity obtained from the depth of the first minimum $\phi = (1+C'D')^{-1}$ gives a value of $\sim$ 75%. The theoretical calculations were tried by assuming an initial value of crystallinity as obtained above and the parameters of the model (ϕ, Δc, Δa) were varied. The theoretically calculated curve is shown in Figure 18 along with the experimental correlation function. The values of the theoretical curve with different terms (relation (4.24)), as a function of distance, are given in Table 7B. As expected in an irradiated sample, a low crystallinity and wider distribution of widths are obtained. The deviation, specially at the first maximum can be interpreted as arising from the changes occurred by irradiation[40]. Irradiation brings about cross-linked regions which could have a higher electron density and thus two-phase model is not quite true. Calculation of correlation function based on more phases will yield better results.

Present analysis is based on the existence of two clear-cut phases - the ordered and disordered ones. Such a demarcation is not always possible and it is likely that a model with continuous variation in electron density would yield better results. This and other limitations of the

present model are discussed in the concluding chapter of the thesis.

Studies of Wool Sample

In this part, we briefly describe our preliminary results on small-angle scattering from Rambouillet 715 sample of wool, washed and soxhlet extracted. It was obtained from the Western Utilization Research Centre, Albany, California. Small-angle X-ray scattering from wool sample is given in Plate 1(c). The microphotometer record of the scattering from wool is shown in Figure 19. The analysis is carried out by a direct comparison between the scattering calculated for certain theoretical models and the scattering actually observed in experiment. It is assumed that the fibres studied have a high degree of orientation, the micro-crystallites being parallel to the fibre axis (nearly so). The scattering obtained consists of a narrow band along the equator of about the same width as the height of the beam (Plate 1(c)). The crystallites may, therefore, be regarded as very long compared to their radius and the wavelength of the radiation. For the calculation, these particles may be considered to have infinite length. The scattering theory used is based on a model consisting of a system of parallel cylindrical rods which scatter either independently or nonindependently and which have nearly constant diameter and homogeneous inner structure.

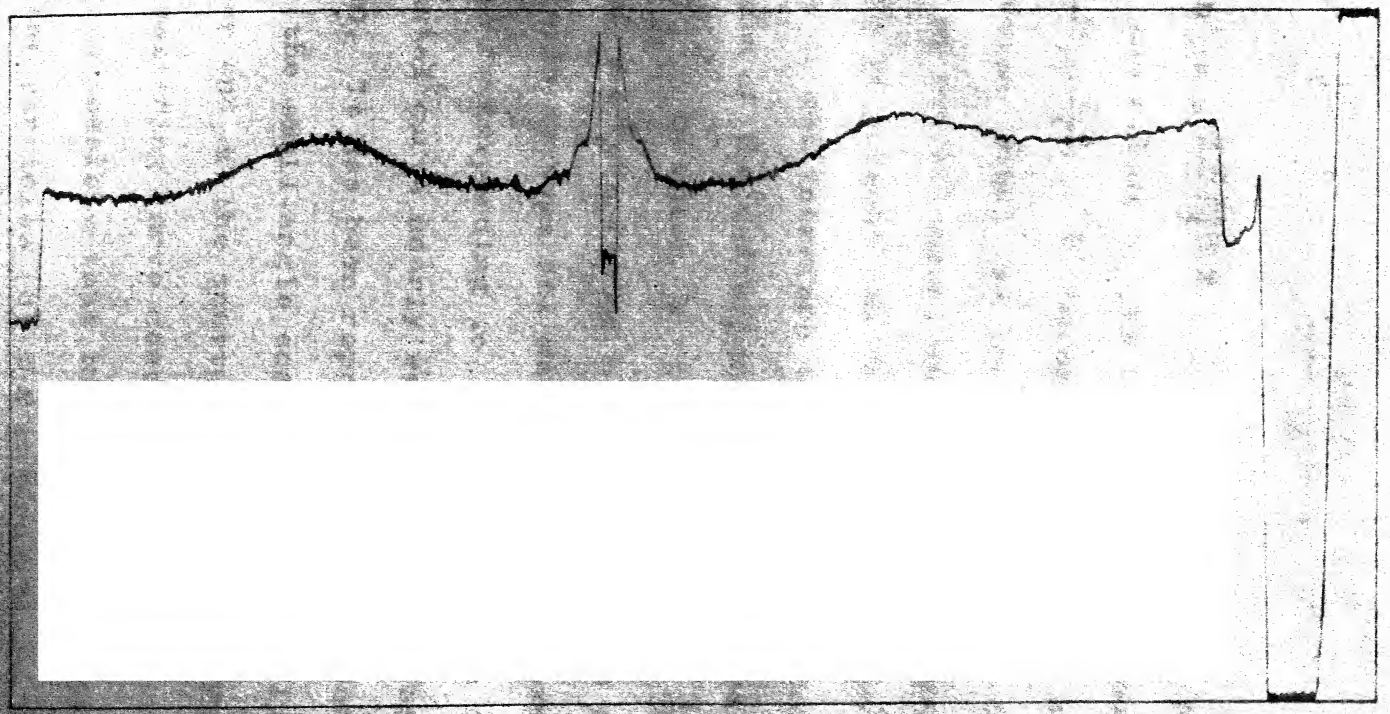

FIG. 19 MICROPHOTOMETER RECORD OF SMALL-ANGLE X-RAY SCATTERING FROM WOOL

The amplitude ϕ scattered by a cylindrical particle is proportional to

$$\frac{2J_1(kR)}{kR}$$

in which $k = \frac{4\pi \sin\theta}{\lambda}$, θ being half the scattering angle and R the radius of the cylinder. For small angles $(\frac{4\pi \sin\theta}{\lambda}) = \frac{2\pi\epsilon}{\lambda}$, ϵ being the scattering angle in radians. The function $\phi(kR)$ is the form factor of the particle. If instead of one cylinder, an assemblage of parallel uniform cylinders is present and the elementary waves from single particle do not interfere then the total scattered radiation is the sum of the radiations from the separate cylinders or $N\left[\phi(kR)\right]^2$ in which N is the number of cylinders. The square of the form factor has been drawn as a function of the angle in radians and matched with the experimental points. The curve corresponding to $R = 45$ Å seems to fit the experimental curve nearly well. These curves are shown in Figure 20. It has been reported that for particles of varying size the small-angle scattering is mostly governed by the higher end of the scattering periodicity. As the tail of the scattering curve does not fit on theoretical curve, it is quite possible that there is (a) distribution in the size of the particles (b) the interparticle interference effects are important. A crude volume filling calculation shows that each microcrystallite unit has approximately

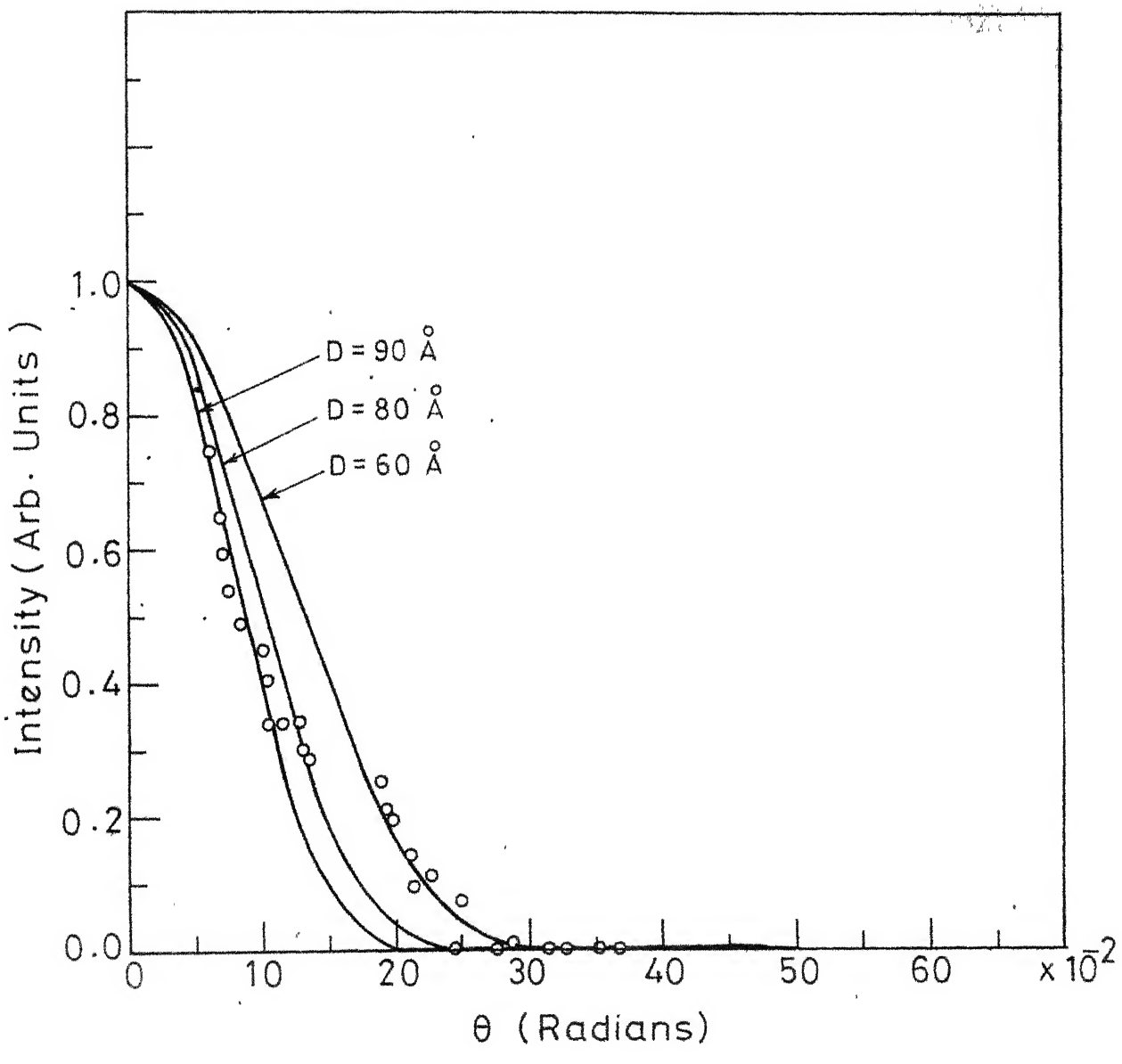

FIG. 20 EXPERIMENTAL POINTS AND THEORETICAL CURVES FOR WOOL SAMPLE

30 alpha helices. An interesting feature of the small-angle scattering is that they vary widely from one member of the Keratin-myosin group to another even though their patterns at wide-angles (i.e. the alpha structure) are closely similar.

Limitations of the present model, specially the effect interparticle interference, are discussed in the next chapter.

REFERENCES

1. G.C. Claver, Jr., R. Buchdahl and R.L. Miller, J. Polymer Sci. 20, 202 (1956).

2. F.R. Anderson, J. Polymer Sci. C3, 123 (1963).

3. E.H. Andrews, J. Polymer Sci. B3, 353 (1965).

4. A. Keller and S. Sawada, Makromol. Chem. 74, 190 (1964).

5. R.P. Palmer and A.J. Cobbold, Makromol. Chem. 74, 174 (1964).

6. P.H. Geil, "Polymer Single Crystals", Interscience Publishers, New York (1963).

7. H.D. Keith, Review article, Kolloid Z. u. Z. Polymere 231, 421 (1969).

8. A. Keller, Review article, Kolloid Z. u. Z. Polymere 231, 386 (1969).

9. A. Keller and A.O'Connor, Nature 180, 1289 (1957).

10. L. Mandelkern, C.R. Worthington and A.S. Posner, Science 127, 1052 (1958).

11. K. Kobayashi and M. Kurokaua, Nature 196, 538 (1962).

12. L. Manderlkern, A.S. Posner, A.G. Diorio and D.E. Roberts, J. Appl. Phys. 32, 1509 (1961).

13. W.O. Statton, J. Polymer Sci. 58, 205 (1962).

14. A. Yu. Zubov, G.S. Markova and V.A. Kargin, Vysokomol. soyed. 5, 1171 (1963).

15. O. Kratky, K. Schwarzkopf and K. Schier, Monatshefte f. Chemie 94, 714 (1963).

16. A. Peterlin in "Small-angle X-ray scattering", Ed. (H. Brumberger), Gordon and Breach, Science Publisher, New York, 1967.

17. T. Seto and Y. Tajima, Jap. J. Appl. Phys. 5, 534 (1966).

18. W.B. Krigbaum, I.Y. Balta and G.H. Via, Polymer 7, 61 (1966).

19. J.M. Schultz, W.J. Robinson and G.M. Pound, J. Polymer Sci. A2, 511 (1967).

20. D. Ya. Tsvakin, Vysokomol. Soedin., Ser A9, 2668 (1967).

21. W.R. Krigbaum and R.W. Godwin, J. Chem. Phy. 43, 4523 (1965).

22. R. Hosemann, W. Wilke and F.J. Balta Calleja, Acta Cryst. 21, 118 (1966).

23. P.H. Geil, J. Polymer Sci. C13, 149 (1966).

24. G. Kortleve and C.G. Vonk, Kolloid Z. u. Z. Polymere 225, 124 (1968).

25. D.R. Buchanann and R.L. Miller, J. Polymer Sci. B5, 771 (1967).

26. V. Luzzati and R. Baro, J. Phys. Rad. 22, 186A (1961).

27. J.W.H. DuMond, Phy. Rev. 72, 83 (1947).

28. A. Guinier and G. Fournet, Nature 160, 501 (1947).

29. O. Kratky, G. Porod and L. Kakovec, Z. Electrochem. 55, 53 (1951).

30. V. Gerold, Acta Cryst. 10, 287 (1957).

31. S. Heine and J. Roppert, Acta Phys. Austriaca, 15, 148 (1962).

32. P. Kent and H. Brumberger, Acta Phys. Austriaca, 17, 263 (1964).

33. W. Ruland, Acta Cryst. 17, 138 (1964).

34. J. Mazur and A.M. Wims, J. Res. Nat. Bur. Stand. 70A, 467 (1966).

35. A.J. Lake, Acta Cryst. 23, 191 (1967).

36. F. Hossfeld, Acta Cryst. 24, 643 (1968).

37. G.R. Strobl, Acta Cryst. A26, 367 (1970).

38. P.W. Schmidt and R. Height, Jr., Acta Cryst. 17, 138 (1964).

39. B. Chu and D.M. Ten Creti, Acta Cryst. 18, 1083 (1965).

40. A. Charlesby, "Atomic Radiation and Polymers", Pergamon Press, New York (1960).

CHAPTER - VI

CONCLUSION

The work outlined in the previous chapters is subject to certain limitations. For example, vibrations of TATNB have been obtained for an isolated molecule though in practice because of the insolubility of TATNB in almost all the solvents, it is just not possible to obtain the spectra in solution form. The experimental data reported here is, thus, obtained in solid form. However, physical state of affairs in a crystalline form is different from the simplified model of isolated molecule. A complete interpretation of the vibrational modes would require calculations on a three dimensional system, taking into account all kinds of intermolecular interactions. The size of the dynamical matrix involved in the solution of vibrational problem of a three-dimensional system is very large and makes the solution of secular equation almost prohibitive.

The general effects on the frequency spectrum to be expected as a result of intermolecular interactions in a crystal can be fairly easily visualised[1]. According to Halford[2] the vibrations of the molecule in the crystalline state are governed by new selection rules derived from site symmetry - a local symmetry around the centre of gravity of a molecule in a unit cell. In general, site symmetry is lower than the molecular symmetry in an isolated state. The change in symmetry may split the degenerate vibrations and

activate optically inactive vibrations. In addition, the spectra obtained in the crystalline state exhibit lattice modes. A more complete analysis including lattice modes can be made by the factor group analysis corresponding to the crystal space group. For a unit cell containing N atoms there will be (3N-3) normal vibrations. For the case of TATNB, where there are two molecules in a unit cell, total number of normal vibrations will be 141 (2x24x3 - 3). The 12 fundamentals known as external vibrations can be further divided into nine rotatory type and three translatory type of oscillations. A complete analysis of factor group fundamentals, however, can be carried out only when the nature of the intermolecular interactions is known.

Assuming a admittedly simplified model of isolated molecule, it has, nevertheless, been possible to find reasonable correlation with observed spectra. Although, interactions through hydrogen-bonds have not been explicitly considered, the adjustment of force constants to obtain agreement with observed frequencies has effectively ta en into account these interactions in a circuitous manner. The force field obtained can be used for similar molecules as a starting point, since the validity of transferability of Urey-Bradley force field has been shown in a series of papers by Scherer[3,4].

Coming to the second part of the thesis, i.e., the work on small-angle scattering of X-rays, the two-phase parallel layer model assumed for polyethylene sample seems to hold to a fair degree. This is seen from the fitting of the major part of the experimental correlation curve with that of the theoretical one. However, small deviations are observed at the first minima. Similar deviations are observed in case of irradiated polyethylene sample where the first maximum is neither well defined nor well matched with the theoretical curve. The situation in irradiated sample is different because irradiation brings about cross-linking[5]. The analysis of the experimental curve is complicated because the cross-linked regions could have a different average electron density than the crystalline and amorphous regions. This will introduce a completely different phase. Irradiation also brings about the broadening of the distribution of layer thicknesses. This suggests that for an irradiated sample a model with more than two phases is needed.

The present analysis of the experimental curve for polyethylene is based on the existence of two clear-cut phases - the ordered and the disordered ones. Such a demarcation is generally not possible. It is likely that a model with continuous variation in electron density at the phase boundaries would yield better results. The correlation

function approach for melt-crystallized polymers has several advantages as indicated in previous chapters. The success of the two-phase model suggests that it can be used for similar systems. Recently, the molecular parameters, such as average length of the crystalline and amorphous phases have been obtained for semicrystalline polymers by making use of the mathematical methods of Markoff chains[6,7]. It would be interesting to compare the present work with such calculations and obtain transition probability of various states. It should be possible to relate these probabilities with the nature of potential barrier around single bonds.

A preliminary analysis of the scattering curve from wool sample is reported in the thesis. The complete analysis has to include interparticle interference which plays an important role in these systems. From the experimental point of view these effects can be removed by swelling the sample in a suitable swelling agent. Further work, taking into account the above factors, is very essential for a fuller interpretation of the experimental results.

REFERENCES

1. G. Zerbi, Appl. Spectroscopy Reviews 2, 193 (1969).

2. H.S. Halford, J. Chem. Phys. 14, 8 (1946).

3. J. Overend and J.R. Scherer, J. Chem. Phys. 32, 1289, 1296 (1960); 33, 446 (1960); 34, 574 (1961).

4. J.R. Scherer and J. Overend, J. Chem. Phys. 32, 1270 (1960); 33, 1681 (1960).

5. A. Charlesby, "Atomic Radiation and Polymers", Pergamon Press, New York (1960).

6. A.V. Tobolsky, J. Chem. Phys. 37, 1193 (1962); A.V. Tobolsky and V.D. Gupta, J. Chem. Phys. 36, 1999 (1962).

7. V.D. Gupta and A.K. Gupta, Proc. Phys. Soc. 90, 1011 (1967).

APPENDIX

SYMMETRY COORDINATES FOR TATNB*

Definition of Internal Coordinates

Stretches	R_1	to	R_6	=	$r(C-C)$
	R_7	to	R_{12}	=	$r(N-O)$
	R_{13}	to	R_{18}	=	$r(N-H)$
	R_{19}	to	R_{21}	=	$r(C-N)_O$
	R_{22}	to	R_{24}	=	$r(C-N)_H$
In-plane angle bendings	R_{25}	to	R_{30}	=	$\phi(C-C-N)_O$
	R_{31}	to	R_{36}	=	$\phi(C-N-O)$
	R_{37}	to	R_{42}	=	$\phi(C-C-N)_H$
	R_{43}	to	R_{48}	=	$\phi(C-N-H)$
	R_{49}	to	R_{51}	=	$\phi(C-C-C)_O$
	R_{52}	to	R_{54}	=	$\phi(O-N-O)$
	R_{55}	to	R_{57}	=	$\phi(C-C-C)_H$
	R_{58}	to	R_{60}	=	$\phi(H-N-H)$
Torsional coordinates	R_{61}	to	R_{66}	=	$t(C-C)$
	R_{67}	to	R_{69}	=	$t(C-N)_O$
	R_{70}	to	R_{72}	=	$t(C-N)_H$
Out-of-plane wagging	R_{73}	to	R_{75}	=	$\omega(O_2N-C)$
	R_{76}	to	R_{78}	=	$\omega(H_2N-C)$
	R_{79}	to	R_{81}	=	$\omega(B-N)_O$
	R_{82}	to	R_{84}	=	$\omega(B-N)_H$

* 'B' represents benzene ring.
r stands for bond stretching, ϕ for in-plane angle bending, t for torsions and ω for out-of-plane wags.

In-plane symmetry coordinates

A_1' Species

(1) $1/\sqrt{6}\ (R_1 + R_2 + R_3 + R_4 + R_5 + R_6)$

(2) $1/\sqrt{6}\ (R_7 + R_8 + R_9 + R_{10} + R_{11} + R_{12})$

(3) $1/\sqrt{6}\ (R_{13} + R_{14} + R_{15} + R_{16} + R_{17} + R_{18})$

(4) $1/\sqrt{3}\ (R_{19} + R_{20} + R_{21})$

(5) $1/\sqrt{3}\ (R_{22} + R_{23} + R_{24})$

(6) $1/\sqrt{6}\ (R_{25} + R_{26} + R_{27} + R_{28} + R_{29} + R_{30})$

(7) $1/\sqrt{6}\ (R_{31} + R_{32} + R_{33} + R_{34} + R_{35} + R_{36})$

(8) $1/\sqrt{6}\ (R_{37} + R_{38} + R_{39} + R_{40} + R_{41} + R_{42})$

(9) $1/\sqrt{6}\ (R_{43} + R_{44} + R_{45} + R_{46} + R_{47} + R_{48})$

(10) $1/\sqrt{3}\ (R_{49} + R_{50} + R_{51})$

(11) $1/\sqrt{3}\ (R_{52} + R_{53} + R_{54})$

(12) $1/\sqrt{3}\ (R_{55} + R_{56} + R_{57})$

(13) $1/\sqrt{3}\ (R_{58} + R_{59} + R_{60})$

A_2' Species

(1) $1/\sqrt{6}\ (R_1 - R_2 + R_3 - R_4 + R_5 - R_6)$

(2) $1/\sqrt{6}\ (R_7 - R_8 + R_9 - R_{10} + R_{11} - R_{12})$

(3) $1/\sqrt{6}\ (R_{13} - R_{14} + R_{15} - R_{16} + R_{17} - R_{18})$

(4) $1/\sqrt{6}\ (R_{25} - R_{26} + R_{27} - R_{28} + R_{29} - R_{30})$

(5) $1/\sqrt{6}\ (R_{31} - R_{32} + R_{33} - R_{34} + R_{35} - R_{36})$

(6) $1/\sqrt{6}\ (R_{37} - R_{38} + R_{39} - R_{40} + R_{41} - R_{42})$

(7) $1/\sqrt{6}\ (R_{43} - R_{44} + R_{45} - R_{46} + R_{47} - R_{48})$

E' Species

(1) $1/\sqrt{12}$ $(2R_1 + 2R_2 \quad R_3 - R_4 - R_5 - R_6)$

(2) $1/\sqrt{12}$ $(2R_1 - 2R_2 - R_3 + R_4 - R_5 + R_6)$

(3) $1/2$ $(R_3 + R_4 - R_5 - R_6)$

(4) $1/2$ $(R_3 - R_4 - R_5 + R_6)$

(5) $1/\sqrt{12}$ $(2R_7 + 2R_8 - R_9 - R_{10} - R_{11} - R_{12})$

(6) $1/\sqrt{12}$ $(2R_7 - 2R_8 - R_9 + R_{10} - R_{11} + R_{12})$

(7) $1/2$ $(R_9 + R_{10} - R_{11} - R_{12})$

(8) $1/2$ $(R_9 - R_{10} - R_{11} + R_{12})$

(9) $1/\sqrt{12}$ $(2R_{13} + 2R_{14} - R_{15} - R_{16} - R_{17} - R_{18})$

(10) $1/\sqrt{12}$ $(2R_{13} - 2R_{14} - R_{15} + R_{16} - R_{17} + R_{18})$

(11) $1/2$ $(R_{15} + R_{16} - R_{17} - R_{18})$

(12) $1/2$ $(R_{15} - R_{16} - R_{17} + R_{18})$

(13) $1/\sqrt{6}$ $(2R_{19} - R_{20} - R_{21})$

(14) $1/\sqrt{2}$ $(R_{20} - R_{21})$

(15) $1/\sqrt{6}$ $(2R_{22} - R_{23} - R_{24})$

(16) $1/\sqrt{2}$ $(R_{23} - R_{24})$

(17) $1/\sqrt{12}$ $(2R_{25} + 2R_{26} - R_{27} - R_{28} - R_{29} - R_{30})$

(18) $1/\sqrt{12}$ $(2R_{25} - 2R_{26} - R_{27} + R_{28} - R_{29} + R_{30})$

(19) $1/2$ $(R_{27} + R_{28} - R_{29} - R_{30})$

(20) $1/2$ $(R_{27} - R_{28} - R_{29} + R_{30})$

(21) $1/\sqrt{12}$ $(2R_{31} + 2R_{32} - R_{33} - R_{34} - R_{35} - R_{36})$

(22) $1/\sqrt{12}$ $(2R_{31} - 2R_{32} - R_{33} + R_{34} - R_{35} + R_{36})$

(23) $1/2$ $(R_{33} + R_{34} - R_{35} - R_{36})$

(24) $1/2$ $(R_{33} - R_{34} - R_{35} + R_{36})$

(25) $1/\sqrt{12}$ $(2R_{37} + 2R_{38} - R_{39} - R_{40} - R_{41} - R_{42})$

(26) $1/\sqrt{12}$ $(2R_{37} - 2R_{38} - R_{39} + R_{40} - R_{41} + R_{42})$

(27) $1/2$ $(R_{39} + R_{40} - R_{41} - R_{42})$

(28) $1/2$ $(R_{39} - R_{40} - R_{41} + R_{42})$

(29) $1/\sqrt{12}$ $(2R_{43} + 2R_{44} - R_{45} - R_{46} - R_{47} - R_{48})$

(30) $1/\sqrt{12}$ $(2R_{43} - 2R_{44} - R_{45} + R_{46} - R_{47} + R_{48})$

(31) $1/2$ $(R_{45} + R_{46} - R_{47} - R_{48})$

(32) $1/2$ $(R_{45} - R_{46} - R_{47} + R_{48})$

(33) $1/\sqrt{6}$ $(2R_{49} - R_{50} - R_{51})$

(34) $1/\sqrt{2}$ $(R_{50} - R_{51})$

(35) $1/\sqrt{6}$ $(2R_{52} - R_{53} - R_{54})$

(36) $1/\sqrt{2}$ $(R_{53} - R_{54})$

(37) $1/\sqrt{6}$ $(2R_{55} - R_{56} - R_{57})$

(38) $1/\sqrt{2}$ $(R_{56} - R_{57})$

(39) $1/\sqrt{6}$ $(2R_{58} - R_{59} - R_{60})$

(40) $1/\sqrt{2}$ $(R_{59} - R_{60})$

Out-of-plane symmetry coordinates

A_1'' Species

(1) $1/\sqrt{6}$ $(R_{61} + R_{62} + R_{63} + R_{64} + R_{65} + R_{66})$

(2) $1/\sqrt{3}$ $(R_{67} + R_{68} + R_{69})$

(3) $1/\sqrt{3}$ $(R_{70} + R_{71} + R_{72})$

A_2'' Species

(1) $1/\sqrt{6}$ $(R_{61} - R_{62} + R_{63} - R_{64} + R_{65} - R_{66})$

(2) $1/\sqrt{3}$ $(R_{73} + R_{74} + R_{75})$

(3) $1/\sqrt{3}$ $(R_{76} + R_{77} + R_{78})$

(4) $1/\sqrt{3}$ $(R_{79} + R_{80} + R_{81})$

(5) $1/\sqrt{3}$ $(R_{82} + R_{83} + R_{84})$

E'' Species

(1) $1/\sqrt{12}$ $(2R_{61} + 2R_{62} - R_{63} - R_{64} - R_{65} - R_{66})$

(2) $1/\sqrt{12}$ $(2R_{61} - 2R_{62} - R_{63} + R_{64} - R_{65} + R_{66})$

(3) $1/2$ $(R_{63} + R_{64} - R_{65} - R_{66})$

(4) $1/2$ $(R_{63} - R_{64} - R_{65} + R_{66})$

(5) $1/\sqrt{6}$ $(2R_{67} - R_{68} - R_{69})$

(6) $1/\sqrt{2}$ $(R_{68} - R_{69})$

(7) $1/\sqrt{6}$ $(2R_{70} - R_{71} - R_{72})$

(8) $1/\sqrt{2}$ $(R_{71} - R_{72})$

(9) $1/\sqrt{6}$ $(2R_{73} - R_{74} - R_{75})$

(10) $1/\sqrt{2}$ $(R_{74} - R_{75})$

(11) $1/\sqrt{6}$ $(2R_{76} - R_{77} - R_{78})$

(12) $1/\sqrt{2}$ $(R_{77} - R_{78})$

(13) $1/\sqrt{6}$ $(2R_{79} - R_{80} - R_{81})$

(14) $1/\sqrt{2}$ $(R_{80} - R_{81})$

(15) $1/\sqrt{6}$ $(2R_{82} - R_{83} - R_{84})$

(16) $1/\sqrt{2}$ $(R_{83} - R_{84})$

SOME OF THE WORK DESCRIBED IN THIS THESIS HAS BEEN PUBLISHED. A LIST OF REFERENCES APPEARS BELOW:

1. V.D. Gupta and B.L. Deopura, 'Low Frequency Neutron Spectrum of 1,3,5-Triamino-2,4,6-trinitrobenzene', Mol. Phys. 19, 589 (1970).
2. B.L. Deopura and V.D. Gupta, 'Vibration Spectra of 1,3,5-Triamino-2,4,6-trinitrobenzene', J. Chem. Phys. (Accepted for publication). 54, 4013 (1971)
3. B.L. Deopura and V.D. Gupta, 'Small-Angle X-Ray Scattering from Polyethylene', Chem. Phys. Letters (Accepted for publication).